Seasonal dynamics in diatom and particulate export fluxes to the deep sea in the Australian sector of the southern Antarctic Zone

Andrés S. Rigual-Hernández, Thomas W. Trull, Stephen G. Bray, Ivia Closset, Leanne K. Armand

Seasonal dynamics in diatom and particulate export fluxes to the deep sea in the Australian sector of the southern Antarctic Zone

Andrés S. Rigual-Hernandez[1*], Thomas W. Trull[2,3], Stephen G. Bray[2], Ivia Closset[4], Leanne K. Armand[1].

1 Department of Biological Sciences, Macquarie University, North Ryde, NSW 2109, Australia

2 Antarctic Climate and Ecosystems Cooperative Research Centre, University of Tasmania, Hobart, Tasmania 7001, Australia

3 CSIRO Oceans and Atmosphere Flagship, Hobart, Tasmania 7001, Australia

4 Sorbonne Universités (UPMC, Univ Paris 06)-CNRS-IRD-MNHN, LOCEAN Laboratory, 4 place Jussieu, F-75005 Paris, France

*Corresponding author (andres.rigualhernandez@mq.edu.au)

Keywords: diatom flux; particulate flux; sediment traps; Southern Ocean.

Abstract

Particle fluxes were recorded over a one-year period (2001-02) in the southern Antarctic Zone in the Australian Sector of the Southern Ocean. Here, we present the results on the seasonal and vertical variability of biogenic particle and diatom valve fluxes. Total mass and diatom fluxes were highly seasonal, with maxima registered during the austral summer and minima during winter. Biogenic opal dominated sedimentation, followed by carbonate, and very low levels of organic carbon (annual average 1.4%). The strong correlation between opal and organic carbon at both depth levels suggests that a significant fraction of organic matter exported to the deep sea was associated with

diatom sedimentation events. Seasonal diatom fluxes appear driven principally by changes in the flux of *Fragilariopsis kerguelensis*. The occurrence of the sea-ice affiliated diatoms *Fragilariopsis cylindrus* and *Fragilariopsis curta* in both sediment traps is considered to correspond to the sedimentation of a diatom bloom advected from an area under the influence of sea ice. Highest fluxes of the subsurface-dwelling species *Thalassiothrix antarctica* registered at the end of the summer bloom were linked to a drop of the light levels during the summer-autumn transition. This study provides the first annual observation on seasonal succession of diatom species in the Australian sector of the Antarctic Zone, and corresponds, in terms of magnitude and seasonality of diatom fluxes, to those in neighbouring sectors (Pacific and eastern Atlantic).

1. Introduction

Diatoms are unicellular algae with an absolute requirement for silicic acid to form their frustules. They constitute a major component of phytoplankton communities, being responsible for ~40% of all marine carbon fixation (Nelson et al., 1995). Diatoms are the main contributors to the silica-rich deposits in deep-sea sediments and are thought to influence the present and past global climate via their influence on the biological pump of CO_2 from the atmosphere into the ocean interior (Nelson et al., 1995; Sarmiento et al., 1998; Matsumoto et al., 2002). The composition of phytoplankton communities and abundance of diatoms within them are related to specific ecological parameters of the water masses where they live (e.g., temperature, sea-ice cover and nutrient availability), and hence in the case of diatoms, their frustules can be used as biotic proxies for palaeoenvironmental and palaeoceanographic reconstructions.

In order to evaluate the role of diatoms in the biological pump and the cycling of silicon, it is essential to thoroughly understand their ecology and the processes that the living biocoenoses undergo from their initial production in the euphotic zone to their eventual preservation in the ocean sediments (e.g. Varela et al., 2004; Grigorov et al., 2014). This knowledge is also required to validate paleorecontructions based on the diatom sedimentary record (e.g. Leventer et al., 1993; Taylor and Sjunneskog, 2002; Armand and Leventer, 2010).

The Southern Ocean is regarded as having one of the highest diatom biomasses of the global ocean. Despite its high-nutrient low chlorophyll (HNLC) regime, massive diatom blooms occur every year during spring and summer associated with specific areas, such as oceanographic fronts (e.g. Honjo et al., 2000; Moore and Abbott, 2002), coastal areas of Antarctica (e.g. Wefer et al., 1988, Bathmann et al., 1991; Arrigo et al., 1999) and the retreating sea ice edge (e.g. Smith and Nelson, 1986; Sullivan et al., 1988). As a result of this relatively high diatom productivity (Pondaven et al., 2000), large amounts of biogenic silica accumulate in the Southern Ocean sediments, mainly south of the Antarctic Polar Front (APF), where about 30% of the global opal marine accumulation occurs (Tréguer and De la Rocha, 2013).

Moored sediment traps are one of the few available tools for monitoring particle fluxes in the open ocean over extended periods of time. They provide a means to determine the magnitude and timing of phytoplankton blooms, document species succession and estimate the remineralization of labile components throughout the water column. The use of sediment traps has contributed significantly to our understanding of diatom ecology in the Southern Ocean and coastal Antarctic systems (e.g. Leventer and Dunbar, 1987; Fischer et al., 1988; Leventer and Dunbar, 1996; Abelmann and Gersonde, 1991; Ishikawa et al., 2001; Suzuki et al., 2001; Pilskaln et al., 2004;

Ichinomiya et al., 2008; Romero and Armand, 2010). However, these studies are scattered in space and time, and large regions of the Southern Ocean, including the Australian Sector, remain undocumented.

During the Australian multidisciplinary ACE CRC SAZ Project (Trull et al., 2001a), the main hydrological zones of the Australian sector of the Southern Ocean were instrumented with sediment trap mooring lines. The central goal of this experiment was to determine the origin, composition and fate of particulate matter transported to the ocean interior. This research yielded important results, including the demonstration that particulate organic carbon (POC) export in the Southern Ocean is similar to the global ocean median (Bray et al., 2000; Trull et al., 2001b).

Here, as part of the ACE CRC SAZ project, we report on the biogenic particle fluxes registered by two sediment traps deployed in the southern Antarctic Zone (60° 44.43´S; 139°E 53.97´S) over a year (November 2001 to September 2002) in order to (1) document the magnitude, composition and seasonal distribution patterns of the settling particle fluxes, with particular focus on diatoms and their specific composition; and (2) assess the effects of dissolution and physical processes in the water column on the diatom assemblage composition by comparing the assemblages registered by the 2000 and 3700 m sediment traps. An improved understanding of diatom ecology and changes that the diatom assemblages undergo during their sinking through the water column should lead to a better interpretation of proxy records in the Southern Ocean.

1.1. Oceanographic setting

The Antarctic Circumpolar Current (ACC) flows eastward around Antarctica driven by strong westerly winds connecting the Pacific, Atlantic and Indian Oceans. Several circumpolar jets or fronts divide the ACC into distinct zones (Fig. 1a), each one

characterized by specific hydrological and biochemical properties (Orsi et al., 1995). The fronts coincide with strong current cores of the ACC defined by contours of sea surface height (SSH). Each of these fronts consists of multiple branches or filaments, where their position varies rapidly over time (Sokolov and Rintoul, 2002, 2007 and 2009a, b). From north to south, these fronts and zones are the Subtropical Front (STF), the Subantarctic Zone (SAZ), the Subantarctic Front (SAF), the Polar Frontal Zone (PFZ), the Polar Front (PF), the Antarctic Zone (AZ) and the Southern ACC Front (SACCF) (Sokolov and Rintoul, 2009a, b).

The surface waters of the Australian sector of the Southern Ocean are nitrate and phosphate rich and their concentrations remain fairly uniform across the ACC (Bostock et al., 2013). In contrast, silicic acid (Si) content shows a marked south to north gradient. Highest Si concentrations are reached south of the Polar Front Zone (up to 70 μM), whereas the Subantarctic Zone waters exhibits low Si values (1 to 5 μM) (Coale et al., 2004; Bostock et al., 2013). Despite the relatively high macronutrient concentrations, Southern Ocean surface waters are often characterized by relatively low phytoplankton biomass. Light limitation related to deep mixing (Sakshaug and Holm-Hansen, 1984) and extremely low concentrations of trace metals such as iron (De Baar et al., 1995; Johnson et al., 1997; Fitzwater et al., 2000; Martin et al., 1990; Boyd et al., 2000) seem to be the main causes for this “high-nitrate, low-chlorophyll” (HNLC) regime.

Sea ice seasonality off East Antarctica is considered linked to patterns of oceanic currents, which in turn are related to sea floor topography (Massom et al., 2013). Seasonal sea-ice advance occurs from early autumn through early spring followed by retreat from late spring through summer (Comiso et al., 1984; Kimura and Wakatsuchi, 2011; Massom et al., 2013).

Our study site, station 61 S (60° 44.43´S; 139°E 53.97´S), is located within the southern Antarctic Zone (AZ-S; Parslow et al., 2001), between the southern branch of the PF (59°S) and the southern front of the SAACF (Rintoul and Bullister, 1999; Rintoul and Sokolov, 2001). The mooring site is within the same region where the first open-ocean iron enrichment experiment in the Southern Ocean (Southern Ocean Iron Release Experiment - SOIREE) was conducted (Boyd et al., 2000) and can be considered representative of the region between the PF and the SACCF (between 54°S and 62°S) (Trull et al., 2001c). Despite surface waters rich in macronutrients (i.e. silicate, phosphate and nitrate), the algal biomass accumulation is considered low (<0.5 μg/L) (Parslow et al., 2001; Popp et al., 1999; Trull et al., 2001c). Copepods, mainly large calanoid copepodites, dominate the zooplankton community at the study site. Grazing pressure is considered low (<1% of the phytoplankton standing stock removed per day) and is thought not to greatly influence the development of the annual bloom (Zeldis, 2001). Very low iron concentrations (0.1-0.2 nM; Sohrin et al., 2000; Boyd et al., 2000) appear to be responsible for the low primary production. The study area is far from the influence of coastal waters and just north of the maximum winter sea-ice extent (Fig. 1b; Massom et al., 2013).

2. MATERIAL AND METHODS

2.1 Field experiment

Site 61 S was instrumented with a mooring line equipped with three McLane Parflux time series sediment traps (Honjo and Doherty, 1988) placed at 1000, 2000 and 3700 m depth in a water column of 4393m (Fig. 1c). Each trap was paired with an Aanderaa current meter and temperature sensor. The trap sampling cups were filled with a buffered solution of sodium tetraborate (1 g L^{-1}), sodium chloride (5 g L^{-1}), strontium

149 chloride (0.22 g L^{-1}), and mercury chloride (3 g L^{-1}). Cup rotation intervals were
150 synchronized between traps and were established based on anticipated mass fluxes. The
151 shortest sampling intervals were 8 days and correspond with the austral summer and
152 autumn, whereas the longest interval was 55 days corresponding with austral winter
153 (Table 1). No samples were recovered from the shallowest trap owing to equipment
154 malfunction. The two deeper traps completed their collection sequence as programmed
155 without any instrumental failures providing a continuous time-series for 317 days
156 (November 30, 2001 to September 29, 2002) divided into 21 collecting intervals. Owing
157 to the low particle fluxes registered at the onset and end of the experiment insufficient
158 material remained for diatom analysis of cup 1 of the 2000 m trap and cups 1, 2, 19, 20
159 and 21 of the 3700 m trap (Table 1). After recovery, sediment trap cups were removed,
160 capped on board and stored at 4°C in the dark until they were processed. The original
161 samples were sieved through a 1mm nylon mesh in order to remove the largest
162 swimmers, and only the fraction <1 mm was analyzed. Then, they were split into 10
163 equal fractions using a McLane WSD-10 wet-sample divider. One complete split was
164 used for microplankton analysis. A detailed description of the geochemical analytical
165 procedures is given by Trull et al. (2001b) and Bray et al. (2000). Component fluxes are
166 reported for individual cups along with average values over the collection or
167 deployment period for each component (Table 1). As the collection period was shorter
168 than a calendar year, annual mean estimates were determined and are presented in Table
169 1. These annual estimates take into account the fact that the unobserved days occurred
170 in winter when fluxes were low, and were obtained by using the flux for the last winter
171 cup (#21 in 2002) to represent mean daily fluxes during the unobserved period.
172 In order to investigate the correlation between time series, a correlation matrix was
173 calculated (Table 2).

174

175 **2.2 Siliceous microplankton sample preparation and analysis**

176 Each diatom fraction sample was refilled with distilled water to 40 ml, from which 10
177 ml was subsampled and buffered with a solution of sodium carbonate and sodium
178 hydrogen carbonate (pH 8) and kept refrigerated for future calcareous nannoplankton
179 analysis. The remaining 30 ml was treated with hydrogen peroxide, potassium
180 permanganate and concentrated hydrochloric acid in order to clean the sample of
181 organic matter and calcareous components following the methodology of Romero et al.
182 (1999, 2000). The resulting sediment slurry was stored in bottles filled with distilled
183 water. Microscopic slides were prepared following the decantation method outlined by
184 Flores and Sierro (1997). This method produces random settling of the diatoms for
185 quantitative microscopic purposes. The dried cover-slip was permanently mounted onto
186 a glass slide with Norland optical adhesive 61 mounting medium (Refractive index:
187 1.56).

188 Qualitative and quantitative analyses were performed using a Olympus BH-2 compound
189 light optical microscope at 1000x magnification with phase-contrast illumination. A
190 minimum of 400 specimens were counted per sample. Each diatom valve was identified
191 to the lowest taxonomic level possible. Scanning Electron Microscope observations of
192 selected samples were used to verify taxonomic identifications made with the LM. The
193 recommendations of Schrader and Gersonde (1978) were used as a basis for the
194 counting of diatom valves. We did not include the counts of the girdle bands of
195 *Dactyliosolen antarcticus* in the determination of relative abundances.

196 The microplankton counts were transformed into daily fluxes of specimens m^{-2} d^{-1}
197 following the formula of Sancetta and Calvert (1988) and Romero et al. (2009):

198

$$F = \frac{Nx \left(\frac{A}{a}\right) x\, V\, x\, S}{d\, x\, T}$$

where “F” is the daily flux of specimens, “*N*” the number of specimens, “A” the total area of a Petri dish, “a” the analysed area, “V” the dilution volume, “S” the split of the cup, “d” the number of days of collection and “T” the aperture area of the sediment trap. The diatom species diversity was estimated applying Shannon’s diversity index (H´) to the relative abundance data ($H' = -\sum p_i \log_2 p_i$, where p = n1/N, n1 = number of specimens of one taxon and N the total number of specimens). Large values of H indicate greater diversity.

The annualized diatom valve flux for the 2000 m sediment trap was estimated following the same procedure as for the component fluxes (Table 1).

The temporal overlap of diatom fluxes between 2000 m and the 3700 m traps occurred between December-May (172 days) (Table 1). This overlap was used to estimate the sinking velocities of diatom valves and to track the alteration of settling diatom assemblages between traps. The sinking settling velocities for the main diatom taxa were calculated from the time lag between associated peaks in both traps and the vertical distance between traps. We used a squared-chord distance as the metric for assessing the similarity between the diatom assemblages of both traps (Ortiz and Mix, 1997). Squared chord distance values can range between 0.0 and 2.0, with 0.0 indicating identical proportions of species within the assemblages being compared.

2.3 Satellite imagery, meteorological and oceanographic data

Weekly mean sea surface temperature (SST) data for the period 2001 to 2002 was extracted from the NOAA Optimum Interpolation Sea Surface Temperature Analysis database (Reynolds et al., 2002). The monthly averages of the upper 300 m thermal

223 structure for the 2001–2002 period (Fig. 2) were obtained for the sampling location
224 from the World Ocean Atlas 2009 (Locarnini et al., 2010). The maximum weekly SST
225 mean during the field experiment was 2.94 °C degrees occurring in March 2002,
226 whereas the minimum was 0.12 °C at the beginning of October 2002. Changes of the
227 weekly mean SST mirrored the seasonal changes in the vertical structure of the water
228 column temperature profile. A pattern of stratification during austral summer months
229 and vertical homogeneity in autumn and winter was noted during the field experiment
230 (Fig. 2).
231 Satellite-derived monthly chlorophyll-*a* concentration and photosynthetically active
232 radiation (PAR) estimates were obtained from NASA's Giovanni program (Acker and
233 Leptoukh, 2007) (Fig. 2). The pigment concentration record was then used as a proxy
234 for surface algal biomass accumulation. The overall chlorophyll-*a* levels were low
235 (0.07-0.30 mg/m^3) and similar to previous observations in the study area (Trull et al.,
236 2001c). The increase in the algal biomass commenced in September 2001 and reached
237 its highest levels in November 2001, coinciding with a maximum in the insolation
238 levels (Fig. 2). Pigment concentration declined through summer and reached its lowest
239 levels in autumn and winter (March to August 2002).
240
241 **3. RESULTS**

242 **3.1 Bulk composition**

243 Total fluxes of particulates at both traps were highly seasonal, with maxima registered
244 during the austral summer (up to 1151 mg m^{-2} d^{-1} at 2000 m and 1157 mg m^{-2} d^{-1} at 3700
245 m) and almost negligible fluxes during winter (up to 42 mg m^{-2} d^{-1} at 2000 m and below
246 detection limits at 3700 m) (Fig. 2). The fluxes of total particulates at 2000 and 3700 m
247 depth showed similar seasonal variations and were closely correlated (R^2 = 0.82; Fig.

4). Particulate fluxes were slightly higher at 2000 m (261 ± mg m^{-2} d^{-1} = deployment average ± standard deviation) than at 3700 m (216 ± 337 mg m^{-2} d^{-1}). Biogenic silica (SiO_2) was the dominant bulk component, regardless of the sampling period or depth (deployment average = 76% at 2000 and 78% at 3700 m). The highest relative contribution of opal was registered from the end of summer through early-autumn at both depths (Table 1). Secondary contributors were carbonate ($CaCO_3$) (7% at 2000 m and 9% at 3700 m) and particulate organic carbon (POC) (1.4% at 2000 m and 1.2% at 3700 m). The relative concentration of carbonate and POC was at its highest in austral spring and summer (Table 1). The fluxes of all components were closely correlated. The results of the correlation matrix are given in Table 2. Total mass flux showed a strong correlation with POC at both sediment traps (R^2 = 0.86 at 2000 m and R^2 = 0.87 at 3700 m). $BSiO_2$ fluxes were also highly correlated with POC at both depths (R^2 = 0.83), whereas $CaCO_3$ and POC fluxes exhibited the lowest values (R^2 = 0.24 at 2000 m and R^2 = 0.63 at 3700 m).

The molar POC/PN ratios were relatively low (Table 1), and thus similar to surface Southern Ocean particles and phytoplankton (Copin-Montegut and Copin-Montegut, 1983).

3.2 Composition of the biogenic opal fraction

The biogenic opal fraction was composed of diatoms, silicoflagellates, radiolarians and the dinoflagellate *Actiniscus pentasterias*. Diatoms were, numerically, the dominant siliceous plankton group registered by the traps with a mean flux between 67 x 10^6 and 76 x 10^6 valves m^{-2} day^{-1} at 2000 m (annualized mean and deployment average, respectively). Mean diatom flux at the 3700 m trap yielded higher values (deployment average = 132 x 10^6 valves m^{-2} day^{-1}) due to the lower sampling duration (172 days) over the winter season (Table 1). Silicoflagellates and radiolarians were three and four

orders of magnitude lower than diatoms (not shown), whereas only one specimen of *A. pentaserias* was indentified in the lower trap. At both depth levels, total diatom fluxes showed strong seasonal variations that closely followed total mass seasonality with Pearson correlation coefficients of r = 0.88 for 2000 m and r = 0.81 for 3700 m (Fig. 4). Diatom frustules from 61 taxa were identified over the entire experiment and are listed in Table 3 together with their relative contribution for the whole sampling period. The seasonal changes in the diatom flux and main species at mooring site 61°S are plotted in Figure 5.

Diversity index values (H´) followed the same seasonal trend as total diatom flux at both depths, with highest values registered during austral summer and lowest during winter (Fig. 5). The squared-chord distance between the sediment trap diatom assemblages at 2000 and 3700 m was 0.003, indicating highly similar proportions of species within depths.

The dominant species of the diatom assemblage was *Fragilariopsis kerguelensis* with a mean flux between 53 x 10^6 and 60 x 10^6 valves m^{-2} day^{-1} at 2000 m (annualized mean and deployment average, respectively). This species contribution ranged from 37% to 96% of the total assemblage at 2000 m (average relative contribution for the overlapping period between traps = 72%; Table 3) and from 31% to 82% at 3700 m (average relative contribution for the overlapping period between traps = 68%) (Table 3). The diatom flux peaks at both depths can be attributed to an increased flux of *F. kerguelensis*, with exception to a peak in late January at 2000 m when *Fragilariopsis pseudonana* dominated the settling assemblage (39%). Secondary contributors to the diatom assemblage at 2000 and 3700 m were *Thalassiosira lentiginosa* (average relative contribution for the overlapping period between traps = 5% and 7%, respectively), *Thalassiosira gracilis* var. *gracilis* (6% and 7%), *Fragilariopsis separanda* (3% and

2%), *Fragilariopsis pseudonana* (4% and 1%), *Fragilariopsis rhombica* (2% and 2%), *Fragilariopsis curta* (1% and 1%) and *Azpeitia tabularis* (1% and 1%) (Table 3 and Fig. 5). It is worth noting that some large and/or entangled frustules of some diatom taxa, such as *Thalassiothrix* (Hallegraeff, 1986), could have been be retained in the 1 mm screen mesh, and therefore, underrepresented in this study.

Scanning electron microscope (SEM) pictures of some of the most relevant taxa are shown in Fig. 6.

3.3 Diatom settling velocities

The calculation of the sinking velocities of the main diatom taxa was only possible for the "particle bloom" period, i.e. from December to March, when distinct peaks were registered in both sediment traps (Fig. 5). The precision of the calculations is limited by the duration of the sampling intervals during this period (8 days). The majority of the taxa exhibited an offset of a single sampling interval (8 days) between the 2000 and 3700 m traps, suggesting and average settling speed of 210 m d^{-1}.

4. DISCUSSION

4.1 Quality check of downward particle fluxes

The use of sediment traps has greatly enhanced our understanding of particle transfer in open ocean environments. However, laboratory and field experiments have shown that the measurement of downward particle fluxes can be subject to several hydrodynamic biases (e.g. Gardner, 1980; Baker et al., 1988, Yu et al., 2001). Therefore, an assessment of the trapping efficiency is needed prior to interpreting the results of any sediment trap experiment.

Our mooring line at site 61°S was maintained taut by the distribution of floats along the line and at the mooring head. Measured mean current speeds at both trap levels were always lower than 10 cm s^{-1} that is, as a rule of thumb, considered the threshold at which trapping efficiency decreases significantly (e.g. Baker et al., 1988, Honjo et al., 1992, Yu et al., 2001, Heussner et al., 2006). On the basis of global comparisons, these conditions suggest that fluxes registered by the traps were unlikely to be significantly biased by under- or over-trapping (Honjo. 1996; Yu et al., 2001).

4.2 Variability of total mass flux and composition of particles

The seasonal variability of the vertical particle transfer at site 61°S appears principally controlled by seasonal changes in the euphotic zone productivity. A significant increase in chlorophyll-*a* concentration from October 2001, approximately two months before any significant warming or stratification occurs (Fig. 2), is in line with an increase in incident insolation from the beginning of spring. Taking into account that pigment concentration at the sea surface reached its highest levels during November 2001 (Fig. 2), and that maximum total particle and diatom fluxes were registered at the beginning of January 2002 (Figs 3 and 5), a time lag of about two months between peak production in the surface waters and onset of particle export in the study area can be assumed. This feature is in agreement with the observations of Buesseler et al. (2001) in the Pacific Sector of the Southern Ocean who reported a similar delay in the delivery of the surface bloom to the ocean interior. Contrastingly, algal biomass reached its annual minimum during the austral winter (June-September) (Fig. 2) and very low particle and diatom export fluxes were registered by the traps (Fig. 3 and 5). These low chlorophyll-*a* concentration and flux values appear to be driven by two factors: (i) insufficient sunlight as a result of the low solar angle and shortened day length that reduced the ability to increase biomass and (ii) intense vertical mixing that transported

phytoplankton below their critical depth, i.e. depth at which the rate of photosynthesis equals the rate of respiration (Fig. 2).

In terms of particle composition, silica-rich and carbonate-poor particulate fluxes registered by the traps mirrored the dominance of diatoms in the waters south of the Antarctic Zone, south of Tasmania. The composition of the settling material is consistent with that of the surface sediments in the region. Opal content in the surface sediments of the Southern Ocean increases from north to south, being the dominant component south of the APF. In contrast, $CaCO_3$ is dominant north of the SAF and decreases southward (Honjo et al., 2000).

Total mass and POC fluxes provided the strongest correlation at both sediment traps (Table 2). As $BSiO_2$ dominated the mass fluxes throughout the sampling period, changes in the $BSiO_2$ flux directly affected POC fluxes, suggesting that diatom valve sedimentation plays an important role in controlling the organic carbon export to depth at the AZ site. On the other hand, the small $CaCO_3$ fluxes and lower correlation values with POC at both sediment traps suggest that $CaCO_3$ had a lesser influence on the POC export. However, as the carrying capacity of POC per $CaCO_3$ unit could not be quantified, the role of $CaCO_3$ in controlling the transfer of organic carbon to depth remains unknown.

4.3 Seasonal trend of diatom fluxes and species composition

The annual diatom fluxes registered by the 2000 m sediment trap (Table 1) fall within the range of those estimated by Fischer et al. (2002) in the AZ of the eastern Atlantic (20×10^6 valves m^{-2} d^{-1}) and those reported by Grigorov et al. (2014) in the Ross Sea Gyre (93×10^6 valves m^{-2} day^{-1}). The diatom fluxes recorded at site 61°S are therefore

371 comparable in magnitude to previously reported diatom data sets of the AZ in the
372 Southern Ocean.
373 Although several factors, such as grazing, dissolution and lateral advection, can
374 influence diatom flux (Boltovskoy et al. 1993), the similar seasonal patterns, with a two
375 month offset between primary productivity and diatom flux variations (Figs. 2 and 5a)
376 suggest that the primary signal of the phytoplankton bloom in the overlying water
377 masses is registered by the traps. About two-thirds of the annual diatom export fluxes at
378 each trap depth were registered during January and February (Fig. 5). A markedly
379 seasonal pattern is characteristic of high latitude systems (e.g. Wefer et al., 1988;
380 Dunbar et al., 1998; Honjo et al., 2000; Fischer et al., 2002; Pilskaln et al., 2004;
381 Romero and Armand, 2010) and illustrates the opportunistic character (r selection) of
382 the dominant species during the summer bloom. As a consequence of this rapid diatom
383 biomass increase, silica in the AZ-S is often stripped out the mixed layer by mid-
384 summer (Trull et al., 2001c).
385 The temporal variations in the composition of diatom assemblages mirrored the changes
386 of the hydrographic conditions in the AZ-S, south of Tasmania. Overall, the major
387 diatom taxa recorded at our mooring site are typical of living and fossil assemblages
388 representing open ocean waters of the Antarctic Zone (Romero and Armand, 2010;
389 Crosta et al., 2005, respectively).
390 The seasonal diatom flux was mainly driven by changes in the flux of the large, heavily-
391 silicified and bloom-forming *F. kerguelensis*, a prominent member of the diatom
392 assemblages in the iron-limited Southern Ocean waters (Smetacek, 1999; Abelmann et
393 al., 2006). Large abundances of *F. kerguelensis* in phytoplankton blooms have also been
394 previously reported in our study area during the SOIREE experiment (Gall et al., 2001;
395 Trull and Armand, 2001), in the AZ of the south-west Atlantic (Hart, 1934) and in the

vicinity of open-ocean fronts in the Atlantic and Pacific sectors (Bathmann et al., 1997; Laubscher et al., 1993; Grigorov et al., 2014). The relative contribution of *F. kerguelensis* at both 61 S traps (68-80%; Table 1) is consistent with its distribution in the Southern Ocean surface sediments where its maximum abundances (70-83%) are found between the Polar Front and the maximum summer sea-ice edge (Crosta et al., 2005). Fischer et al. (2002) and Grigorov et al. (2014) reported lower relative abundance and fluxes of this species in sediment traps in the AZ of the Atlantic sector (29%; 6 x 10^6 valves m^{-2} d^{-1}) and in the Ross Sea Gyre (22%; 20 x 10^6 valves m^{-2} d^{-1}), respectively. However, these sites were under the influence of seasonal ice, where sea-ice affiliated taxa such as smaller *Fragilariopsis* species and *Chacetoceros* spp., are known to often dominate the diatom assemblages (Armand et al., 2005).

At the onset of the summer particle "bloom", H´ rises significantly due to the burst of reproduction and sedimentation of most of the diatom taxa (Fig. 5a). The small and rapidly dividing diatoms *Chaetoceros* group, *Fragilariopsis pseudonana*, *Fragilariopsis rhombica*, *Fragilariopsis separanda* and *Pseudo-nitzschia* spp., together with the cool open ocean species *Thalassiosira gracilis*, are major contributors to the bulk of the spring-summer maximum (Fig. 5). The majority of these diatoms correspond to the Group 1 defined by Quéguiner (2013), consisting of slightly silicified and fast-growing species that undergo rapid species succession during productive periods. The biomass accumulation of such diatoms is thought to be controlled principally by nutrient availability rather than grazing pressure. This concept agrees well with the observations of Zeldis (2001) who reported low grazing impact over the bloom development during the SOIREE experiment. At the end of their growth season, these bloom-forming species are considered to undergo mass mortality resulting in the formation of aggregates that rapidly sink from the euphotic zone (Assmy et al., 2013).

The AZ-S site is remote from the direct influence of sea-ice in summer (Massom et al., 2013; Fig. 1b), which makes the occurrence of the sea-ice affiliated diatoms *Fragilariopsis cylindrus* and *Fragilariopsis curta* during January (Fig. 5b) puzzling. The distribution of *F. cylindrus* in the modern Southern Ocean is constrained to the north by the maximum summer sea ice edge (Semina, 2003; Armand et al., 2005; Esper et al. 2010), whereas *F. cylindrus* appears limited by the maximum extension of sea ice during winter (Armand et al., 2005; Esper et al., 2010). Likely explanations for the presence of these species at site 61°S are either (i) the occurrence of an iceberg in the vicinity of our study area or (ii) the advection of a transient bloom produced in a region under the influence of sea ice. Rich sea-ice affiliated diatom communities have been found in association with free-drifting icebergs (e.g. Smith et al., 2011), however this explanation is unlikely since our site is remote from any known iceberg pathway (Gladstone et al., 2001). Taking into account a time lag of about two months between peak production and particle export, a healthy and neutrally buoyant bloom could cover a much larger distance than that estimated for a sinking particle (detailed in 4.5). Sea-ice coverage west of ~90°E can reach latitudes well above 61°S (Massom et al., 2013; Fig. 1b). We hypothesize that the pulses of *F. curta* and *F. cylindrus* could correspond to the sedimentation of a diatom bloom that was either advected from an area upstream the ACC under the influence of seasonal sea ice or transported northward by Antarctic Surface Water currents (AASW) produced by the seasonal retreat of the sea ice, south of our study.

Enhanced fluxes of the large and thick-walled *F. kerguelensis* persisted for a longer period (until April) than those of Group 1 (sensu Quéguiner, 2013) most likely contributing to the progressive reduction of silicic acid concentrations in the mixed layer throughout the summer. A similar pattern was reported by Assmy et al. (2013)

both inside and outside the iron-fertilized bloom during the European Iron Fertilization Experiment (EIFEX). *Fragilariopsis kerguelensis* is considered a "sinking-silica species" (Assmy et al., 2013) largely responsible for the decoupling of silicon and carbon cycles in the iron-limited ACC.

At the end of the diatom export maximum (i.e. February-March), *Thalassiothrix antarctica* contributed more significantly to the flux via increased abundances (Fig. 5b). This species is a large, slow-growing diatom distributed within discrete layers of the water column (Kemp et al., 2000). Such diatoms are considered k-strategists (Kemp and Villareal, 2013) and fall within Group 2 defined by Quéguiner (2013). High abundances of *Thalassiothrix antarctica* have been reported within and south of the APF (Laubscher et al., 1995; Bracher et al., 1999) and associated to a subsurface chlorophyll maximum in the PFZ south of Tasmania (Kopczynska et al., 2001; Parslow et al., 2001; Gomi et al., 2010) and in Prydz Bay (Quilty et al., 1985). We suspect that *Thalassiothrix antarctica* develops in parallel to Group 1 diatoms, as a result of them inhabiting the pycnocline discontinuity, exploiting deep nutrients and undergoing low rates of primary productivity under low-light conditions (Kemp et al., 2000, 2006; Quéguiner, 2013). The abrupt drop of the photosynthetically active radiation levels to less than half their peak values from February to March (Fig. 2a) and/or the occurrence of a vertical mixing event may have produced both light and/or nutrient limitation leading to the rapid flocculation and sinking of *T. antarctica* during the summer-autumn transition.

Post-March diatom export decreases significantly (Fig. 5a) due to the reduction to lowest levels of light and the concomitant intensification of mixing of the water column (Fig. 2a,b). The "post-bloom" diatom assemblage is characterized by low diversity values (Fig. 5a) mainly due to the high relative abundance of *F. kerguelensis* (up to 96% in September). The remaining assemblage is subsequently composed of large and

heavily silicified centrics such as *Thalassiosira lentiginosa, Azpeitia tabularis* and *Thalassiosira oliveriana.* These are typical open ocean diatoms (Crosta et al., 2005; Romero et al., 2005) with presumed lower nutrient requirements than the summer bloom-forming species.

4.4 Transfer to depth

Our results suggest that a fast and relatively undisturbed downward transport of particles occurred between 2000 and 3700 m (Fig. 3 and 4). The similar BSi and POC content in both traps (Table 1) indicates that little silica dissolution and remineralization occurred between 2000 and 3700 m. Such a result is consistent with previous sediment trap studies that reported minimal alteration of the silica and organic carbon fluxes below the mesopelagic-bathypelagic boundary (~2000 m) (Takahashi, 1986; Honjo et al., 2009). However, the high Si/C at both depth levels also implies that organic matter is recycled faster than opal before reaching the traps, and this must occur at mesopelagic depths. We interpret this as the remineralization of the settling material by the microbial community and by the zooplankton that preferentially feed on organic matter (Honjo, 2009). High Si/C ratios are characteristic of the iron-limited systems of the Southern Ocean where large and highly silicified species (e.g. *Fragilariopsis kerguelensis*) dominate the diatom assemblages. In this regard, the average POC content (1.4%) of our samples at 2000 m is very low, and the average BSi/POC molar ratio for the entire collection period was less than 0.1 for both traps, in comparison to an average of ~1 for a compilation of deep Southern Ocean traps (Honjo et al., 2008) and a median of ~2 for a global compilation (Lampitt and Antia, 1998). This makes it clear that the trap samples have experienced very strong losses of organic carbon, consistent with previous

studies suggesting that Southern Ocean waters south of the Polar Front can be described as low carbon export regimes (Lam and Bishop, 2007).

The sinking velocities of the major diatom taxa during the "particle bloom" indicate rapid sedimentation of the diatom assemblages between the upper and lower traps (210 m d^{-1}). These settling speeds are very similar to those estimated by Honjo et al. (2000) in the AZ of the Pacific Sector and are equal, or greater than, those observed in high productivity areas at lower latitudes (Honjo, 1996). In contrast, based on the time delay between samples with similar silicon isotopic signatures at different depths at site 61 S, Closet et al. (unpublished results) estimated the settling velocities outside the production period to be 120 m d^{-1} or less. These observations suggests that sinking rates of diatom valves at site 61 S are related to flux size, perhaps because higher fluxes lead to the formation of fast-sinking aggregates (e.g. Alldredge and Gotschalkt, 1989). This concept is consistent with the observations of Grigorov et al. (2014) on sediment trap material from the Pacific Sector of the Southern Ocean who reported abundant diatom aggregates at times of peak flux and mainly individual cells and small chains outside the production period. Moreover, the formation of aggregates would also explain the enhanced POC export (Table 1) in association with high fluxes of Group 1 diatoms during the production period (Assmy et al., 2013).

The pulse of *Thalassiothrix antarctica* in early March at both depths coincides with an upturn of the POC fluxes (Table 1). *Thalassiothrix antarctica* cells are about 60 times larger (in estimated biovolume) than *F. kerguelensis* (Cornet-Barthaux et al., 2007), and therefore, have the potential to contribute significantly to the annual organic carbon export even at background concentrations (Goldman 1993; Goldman and McGillicuddy, 2003; Quéguiner et al., 2013).

519 During winter, the lower sinking rates and high area/volume ratios of single diatom
520 cells may facilitate the recycling of the valves and remineralization of organic matter in
521 the upper water column. The enrichment of dissolution-resistant diatoms (e.g.
522 *Fragilariopsis kerguelensis*, *Thalassiosira oliveriana*, *Azpeitia tabularis*) during the
523 winter months observed in our traps could, therefore, be partially related to enhanced,
524 selective dissolution of more lightly silicified species (e.g. *Pseudo-nitzschia* spp.,
525 *Fragilariopsis pseudonana*, *Chaetoceros* spp.).
526 With regard to the comparison of the annual diatom assemblage between traps, their
527 highly similar abundance proportions, as revealed by the low squared chord distance
528 score, indicate that both traps registered diatom assemblages from the same source.
529 Moreover, the latter results further support the idea that silica BSi dissolution below
530 2000 m is minimal at the AZ-S site.
531

532 **CONCLUSIONS**

533 The main objective of our study was to document the variability in the magnitude,
534 timing and composition of particle and diatom export fluxes to the deep sea in the
535 southern Antarctic Zone (AZ-S) within the Australian sector of the Southern Ocean. To
536 examine this issue, we studied the year-round dynamics of particle flux from November
537 2001 through September 2002. The overall fluxes of biogenic particles to the mid- and
538 deep water column in the AZ-S were markedly seasonal with peak fluxes occurring
539 during the austral summer and very low export during winter. This seasonal pattern is
540 mediated by algal productivity. Comparison of satellite and particle flux data suggests a
541 delay of about two months between peak production and onset of particle export. The
542 biogenic opal fraction largely dominates the export throughout the year, and is mainly
543 delivered by diatoms. Carbonate and organic carbon are secondary components.

Diatom seasonal fluxes followed the seasonality of the biogeochemical particle fluxes at both depths and their magnitude (67-76 x 10^6 valves m^{-2} day^{-1}) is similar to previously published data recorded in the AZ of other sectors of the Southern Ocean. The diatom assemblages recovered at our mooring site are typical of the open ocean waters of the Antarctic Zone (Crosta et al., 2005) and their seasonal succession agrees well with the conceptual scheme proposed by Quéguiner (2013) for the POOZ (Permanently Open Ocean Zone) and the PFZ (Polar Frontal Zone). *Fragilariopsis kerguelensis* is, by far, the most dominant diatom species in the sediment trap samples. The occurrence of the sea-ice affiliated species *F. cylindrus* and *F. curta* may correspond to the sedimentation of a diatom bloom advected from an area under the influence of sea ice upstream the ACC. The sedimentation pulse of the deep-dwelling species *Thalassiothrix antarctica* during the February-March transition appears to have been triggered by an abrupt drop of the light levels and/or a vertical mixing event.

Finally, the good correlation between the total mass fluxes at both sediment traps and their similar diatom species composition suggests fast and undisturbed settling of particles through the deep water column at the AZ-S site.

Acknowledgements

This project is supported through funding from the Australian Government´s Australian Antarctic Science Grant Program (Project number 4078) and Macquarie University. The SAZ Project is grateful for logistical and equipment support from ANARE and the Australian Antarctic Division (T. Trull, ASAC grants 1156 and 2256), the CSIRO Division of Marine Research Oceans and Climate Program, Geosciences Australia, and New Zealand's National Institute of Water and Atmospheric Research (NIWA). The officers, crews, and scientific staff of the Aurora Australis voyages are thanked for their

professionalism and dedication. Anne-Marie Ballegeer is greatly acknowledged for her comments during the preparation of the manuscript. The authors acknowledge the assistance and support of Nicole Vella and Debra Birch from the Macquarie University Microscopy Unit for performing scanning electron microscopy experiments. Robert O'Malley provided remote sensing support during analysis. The chlorophyll-*a* data used in this paper were produced with the Giovanni online data system, developed and maintained by the NASA GES DISC. Dr Anne-Marie Ballegeer is acknowledged for her suggestions and technical support. Critical comments and suggestions from two anonymous reviewers helped to improve the manuscript.

FIGURE CAPTIONS

Figure 1. a. Location of the sediment trap mooring line in the Antarctic Zone of the Australian sector of the Southern Ocean. Fronts (STF - Subtropical Front, SAF - Subantarctic Front, PF - Polar Front, SB - Southern Boundary), regions (STZ – Subtropical Zone, SAZ – Subantarctic Zone, PFZ – Polar Front Zone, ACC – Antarctic Zone and SACCZ - Zone south of the ACC) and maximum extension of winter sea ice (Max WSI) are shown. Triangle represents the position of 61°S mooring during the experiment (Nov. 2001 – Sep. 2002). **b.** Mean sea ice season duration map for the East Antarctic sector (1979/80-2009/10), with contours for 100, 200 and 300 days marked (modified from Massom et al., 2013). **c.** Schematic diagram of the Australian sector of the Southern Ocean depicting the bathymetry, main water masses and mooring configuration. SAMW – Subantarctic Mode Water, AAIW – Antarctic Intermediate Water, UCDW – Upper Circumpolar Deep Water, LCDW – Lower Circumpolar Deep Water and AABW – Antarctic Bottom Water. Figure is adapted from Bostock et al. (2013).

Figure 2: (**a**) Monthly mean chlorophyll-*a* concentration (mg m^{-3}), sea surface temperature (SST) (°C) and photosynthetically active radiation (Einstein m^{-2} d^{-1}) for the period November 2001 to September 2002. No data was available from April to August in 2001 and 2002. (**b**) Seasonal variation in the vertical structure of temperature (°C) at the 61°S site.

Figure 3. Temporal variability of the total mass and major biogenic fluxes for <1 mm fraction at 2000 and 3700 m water depth from November 2001 through to November 2002 at the 61°S site.

Figure 4. Correlation between (a) mass flux (mg m^{-2} day^{-1}) at 2000 and 3700 m, and (b) mass flux (mg m^{-2} day^{-1}) and diatom valve flux (10^6 m^{-2} day^{-1}) at 2000 and 3700 m.

Figure 5. Seasonal variation of (a) total diatom flux and Shannon's diversity index (H´) and (b) flux and relative abundance of the main diatom species at 2000 and 3700 m sediment traps. The arrows indicate the associated peaks of valve flux at both depths used to calculate the sinking velocities.

Figure 6: SEM photos of some of the most relevant diatom taxa collected by the sediment traps at site 61°S. (a) *Azpeitia tabularis*. (b) *Chaetoceros atlanticus* (resting stage). (c) *Fragilariopsis curta*. (d) *Fragilariopsis cylindrus*. (e) *Fragilariopsis kerguelensis*. (f) *Fragilariopsis pseudonana*. (g) *Fragilariopsis rhombica*. (h) *Fragilariopsis separanda*. (i) *Pseudo-nitzschia* spp. (j) *Thalassiosira gracilis* var.

gracilis. (k) *Thalassiosira lentiginosa*. (l) *Thalassiothrix antarctica*. Scale bars: d, f = 1 μm; h, i = 2 μm; c, e, j = 5 μm; a, b, g, k, l = 10 μm.

Table 1: Daily export fluxes of total mass flux, biogenic silica ($BSiO_2$), calcium carbonate ($CaCO_3$), particulate organic carbon (POC) and diatom valves registered at the 61°S site from November 2001 through October 2002. Mass fluxes listed as zero were too small to measure (<1 mg). *Average diatom fluxes for the 2000 and 3700 m traps have been estimated for different sampling intervals (309 and 172 days, respectively).

Table 2: Correlation matrix (R^2) for the total mass and bulk compound fluxes at both sediment traps.

Table 3: Integrated fractional abundances of the diatom taxa found at the 2000 and 3700 m sediment traps at station 61°S.

REFERENCES

Abelmann, A., Gersonde, R. (1991) Biosiliceous particle flux in the Southern Ocean, *Mar. Chem.*, **35**, 503—536.

Abelmann, A., Gersonde, R., Cortese, G., *et al.* (2006) Extensive phytoplankton blooms in the Atlantic Sector of the glacial Southern Ocean, *Paleoceanography*, **21**, PA1013

Acker, J.G. and Leptoukh, G. (2007) Online analysis enhances use of NASA Earth science data. *Eos, Transactions*. AGU, **88**, 14–17.

643

644 Alldredge, A.L., Gotschalkt, C.C. (1989) Direct observations of the mass flocculation of
645 diatom blooms: characteristics, settling velocities and formation of diatom aggregates.
646 *Deep-Sea Res. (1 Oceanogr. Res. Pap.)*, **36** (2), 159–17

647

648 Arrigo, K.R., Robinson, D.H., Worthen, D.L., *et al.* (1999) Phytoplankton community
649 structure and the drawdown of nutrients and CO_2 in the Southern Ocean. *Science* **283**,
650 365–367.

651

652 Armand, L.K., Crosta, X., Romero, O.E. *et al.* (2005) The biogeography of major diatom
653 taxa in Southern Ocean surface sediments: 1. Sea ice related species. *Paleogeogr.,*
654 *Palaeoclimatol., Palaeoecol.,* **223**, 93–126.

655

656 Armand, L.K., Leventer, A. (2010) Palaeo sea ice distribution and reconstruction derived from the
657 geological record. In *Sea Ice*, (Eds. D. N. Thomas & G.S. Dieckmann, G.S.), pp. 469-530,
658 Wiley-Blackwell Publishing Ltd, Oxford.

659

660 Assmy, P., Smetacek, V., Montresor, M. (2013) Thick–shelled, grazer–protected diatoms
661 decouple ocean carbon and silicon cycles in the iron–limited Antarctic Circumpolar
662 Current. *PNAS* **110** (51) 20633–20638.

663

664 Baker, E.T., Milburn, H.B., Tennant, D.A. (1988) Field assessment of sediment trap
665 efficiency under varying flow conditions. *J. Mar. Res.* **46**, 573–592.

666

667 Bathmann, U., Fischer, G., Müller, P.J. *et al.* (1991) Short–term variations in particulate
668 matter sedimentation off Kapp Norvegia, Weddell Sea, Antarctica: relation to water

669 mass advection, ice cover, plankton biomass and feeding activity. *Polar Biol.* **11**, 185–
670 195.
671
672 Boltovskoy, D., Alder, V.A., Abelmann, A. (1993) Annual flux of Radiolaria and other
673 shelled plankters in the eastern equatorial Atlantic at 853 m: seasonal variations and
674 polycystine species-specific responses. *Deep-Sea Res. (1 Oceanogr. Res. Pap.)*, **40**(9),
675 1863–1895.
676
677 Bostock, H.C., Barrows, T.T., Carter, L. et al. (2013) A review of the Australian–New
678 Zealand sector of the Southern Ocean over the last 30 ka (Aus-INTIMATE project).
679 *Quat. Sci. Rev.* **74**, 35–57.
680
681 Boyd, P., Watson, J., Law, C.S. *et al.* (2000) Phytoplankton bloom upon mesoscale iron
682 fertilisation of polar Southern Ocean waters. *Nature* **407**, 695–702.
683
684 Bracher, A.U., Kroon, B.M.A., Lucas, M.I. (1999) Primary production, physiological
685 state and composition of phytoplankton in the Atlantic Sector of the Southern Ocean.
686 *Mar. Ecol. Pro. Ser.* **190**, 1–16.
687
688 Bray, S., Trull, T.W., Manganini, S. (2000) SAZ Project Moored Sediment Traps: Results
689 of the 1997–1998 Deployments, 128 pp, Antarct. Coop. Res. Cent., Hobart, Tasmania,
690 Australia.
691
692 Buesseler, K.O., L. Ball, J. Andrews, *et al.*, (2001) Upper ocean export of particulate
693 organic carbon and biogenic silica in the Southern Ocean along 170°W. *Deep-Sea Res.*

694 *(2 Top. Stud. Oceanogr.)* **48** (19–20), 4275–4297.
695
696 Coale, K.H., Johnson, K.S., Chavez, F.P., *et al.* (2004) Southern Ocean iron enrichment
697 experiment: Carbon cycling in high- and low-Si waters. *Science* **304** (5669), 408–414.
698
699 Comiso, J.C., Zwally, H.J. (1984) Concentration gradients and growth/decay
700 characteristics of the seasonal sea ice cover. *J. Geophys. Res*. **89**, 8081–8103.
701
702 Copin-Montegut, C., Copin-Montegut, G. (1983) Stoichiometry of carbon, nitrogen, and
703 phosphorus in marine particulate matter. *Deep-Sea Res. (1 Oceanogr. Res. Pap.)*, **30** (1),
704 31–46.
705
706 Cornet-Barthaux, V., Armand, L.K., Quéguiner, B. (2007) Biovolume and biomass
707 measurements of key Southern Ocean diatoms. *Aquat. Microb. Ecol.* **48** (3), 295–308.
708
709 Crosta, X., Romero, O., Armand, L.K., *et al.* (2005) The biogeography of major diatom
710 taxa in Southern Ocean sediments: 2. Open ocean related species. *Palaeogeogr.*,
711 *Palaeoclimatol.*, *Palaeoecol.*, **223**, 66–92.
712
713 De Baar, H.J.W., de Jong, J.T.M., Bakker, D.C.E. *et al.* (1995) Importance of iron for
714 phytoplankton blooms and carbon dioxide drawdown in the Southern Ocean. *Nature*
715 **373**, 412–415.
716

717 Dunbar, R.B., Leventer, A.R. and Mucciarone, D.A. (1998) Water column sediment
718 fluxes in the Ross Sea, Antarctica: atmospheric and sea ice forcing. *J. Geophys. Res.*
719 **103** (30) 741–59
720
721 Esper, O., Gersonde, R., Kadagies, N. (2010). Diatom distribution in southeastern Pacific
722 surface sediments and their relationship to modern environmental variables.
723 *Palaeogeogr., Palaeoclimatol., Palaeoecol.,* 287, 1–27.
724
725 Fischer, G., Fütterer, D., Gersonde, R., *et al.* (1988) Seasonal variability of particle flux in
726 the Weddell Sea and its relation to ice cover. *Nature*, **335**, 426–8.
727
728 Fischer, G., Gersonde, R., Wefer, G. (2002) Organic carbon, biogenic silica and diatom
729 fluxes in the marginal winter sea-ice zone and in the Polar Front Region: interannual
730 variations and differences in composition. *Deep-Sea Res. (2 Top. Stud. Oceanogr.),* **47**,
731 1721–1745.
732
733 Fitzwater, S.E. Johnson, K.S., Gordon, *et al.* (2000) Trace metal concentrations in the
734 Ross Sea and their relationship with nutrients and phytoplankton growth. *Deep-Sea Res.*
735 *(2 Top. Stud. Oceanogr.),* **47**, 3159–3179.
736
737 Flores, J.A., Sierro, F.J. (1997) A revised technique for the calculation of calcareous
738 nannofossil accumulation rates. *Micropal.*, **43**, 321–324.
739
740 Gall, M.P., Boyd, P.W., Hall, J., *et al.* (2001) Phytoplankton processes. Part 1:
741 Community structure during the Southern Ocean Iron Release Experiment (SOIREE)

Deep-Sea Res. (1 Oceanogr. Res. Pap.), **48**, 2551–2570.

Gardner, W.D. (1980) Sediment trap dynamics and calibration: a laboratory evaluation. *J. Mar. Res.*, **38**, 17–39.

Gardner, W.D. (1985). The effect of tilt on sediment trap efficiency. *Deep-Sea Res. (1 Oceanogr. Res. Pap.)* **32**, 349–361.

Gladstone, R.M., Bigg, G.R., Nicholls, K.W. (2001) Iceberg trajectory modelling and meltwater injection in the Southern Ocean. *J. Geophys Res.*, **106** (9), 19903–19915.

Goldman, J.C. (1993) Potential role of large oceanic diatoms in new primary production. *Deep-Sea Res. (1 Oceanogr. Res. Pap.)* **40** (1), 159–168.

Goldman, J.C., McGillicuddy, D.J. (2003) Effect of large marine diatoms growing at low light on episodic new production. *Limnol. Oceanogra.*, **48** (3), 1176–1182.

Gomi, Y., Fukuchi, M., Taniguchi, A. (2010) Diatom assemblages at subsurface chlorophyll maximum layer in the eastern Indian sector of the Southern Ocean in summer. *J. Plank. Res.* **32** (7), 1039–1050.

Grigorov, I., Rigual-Hernandez, A.S., Honjo, S., *et al.* (2014) Settling fluxes of diatom frustules to the interior of the Antarctic Circumpolar Current along 170^{o}W. *Deep-Sea Res. (1 Oceanogr. Res. Pap.)*, **93**, 1-13.

767 Hallegraeff, G.M. (1986) Taxonomy and morphology of the marine plankton diatoms
768 *Thalassionema* and *Thalassiothrix*. Diatom Research, **1**, 57-80.
769
770 Hart, T. (1934) On the phytoplankton of the South-West Atlantic and the Bellinghausen
771 Sea, 1929–31. *Discovery Reports*, **8**, 1–268.
772
773 Heussner, S., Durrieu De Madron, X., Calafat, A. *et al.* (2006) Spatial and temporal
774 variability of downward particle fluxes on a continental slope: Lessons from an 8-yr
775 experiment in the Gulf of Lions (NW Mediterranean) *Mar. Geol.*, **234**, 63–92.
776
777 Honjo, S. (1996) Fluxes of particles to the interior of the open oceans, in Particle Flux in
778 the Ocean, edited by V. Ittekkot *et al.*, pp. 91–154, John Wiley, New York.
779
780 Honjo, S. (2009) Biological pump and particulate fluxes. In: Steele, J.H., Thorpe, S.A.,
781 Turekian, K.K. (Eds.) *Encyclopaedia of ocean sciences*. Academic Press, San Diego,
782 CA, 371–375
783
784 Honjo, S., Doherty, K.W. (1988) Large aperture time-series sediment traps; design
785 objectives, construction and application. *Deep-Sea Res.* **35**(1), 133–149
786
787 Honjo, S., Francois, R., Manganini, S., *et al.* (2000) Particle fluxes to the interior of the
788 Southern Ocean in the Western Pacific sector along 170 degrees W. *Deep-Sea Res. (2*
789 *Top. Stud. Oceanogr.),* **47** (15–16), 3521–3548.
790

Honjo, S., Manganini, S.J., Krishfield, R.A. *et al.* (2008) Particulate organic carbon fluxes to the ocean interior and factors controlling the biological pump: A synthesis of global sediment trap programs since 1983. *Progr. Ocean.*, **76** (3), 217–285.

Honjo, S., Spencer, D.W., Gardner, W.D. (1992) A sediment trap intercomparison experiment in the Panama Basin, 1979. *Deep-Sea Res. (1 Oceanogr. Res. Pap.)* **39**, 333–358.

Ichinomiya, M., Gomi, Y., Nakamachi, M., *et al.* (2008) Temporal variations in the abundance and sinking flux of diatoms under fast ice in summer near Syowa Station, East Antarctica. *Polar Science*, **2**, 33–40.

Ishikawa, A., Wasiyama, N., Tanimura, A., *et al.* (2001) Variation in the diatom community under fast ice near Syowa Station, Antarctica, during the austral summer of 1997/98. *Polar Bioscience*, **14**, 10–23.

Johnson, K.S., Gordon, R.M. and Coale, K.H. (1997) What controls dissolved iron concentrations in the world ocean?. *Mar. Chem.*, **57** (3–4), 137-161.

Kemp, A.E.S., Pike, J., Pearce, R.B. *et al.* (2000) The "Fall dump" a new perspective on the role of a "shade flora" in the annual cycle of diatom production and export flux. *Deep-Sea Res. (1 Oceanogr. Res. Pap.)*, **47**, 2129–2154.

814 Kemp, A.E.S., Pearce, R.B., Grigorov, I. (2006) Production of giant marine diatoms and
815 their export at oceanic frontal zones:implications for Si and C flux from stratified
816 oceans. *Global Biogeochem. Cycles* **20** (4), GB4S04.
817
818 Kemp, A.E.S., Villareal, T.A. (2013) High diatom production and export in stratified
819 waters – A potential negative feedback to global warming. *Progr. Ocean.*, **119** (0), 4–
820 23.
821
822 Kimura, N., Wakatsuchi, M. (2011) Large-scale processes governing the seasonal
823 variability of Antarctic sea-ice area. *Tellus* **63A**, 828–840.
824
825 Kopczynska, E.E., Dehairs, F., Elskens, M. *et al.* (2001) Phytoplankton and
826 microzooplankton variability between the Subtropical and Polar Fronts south of
827 Australia: Thriving under regenerative and new production in late summer. *J. Geophys.*
828 *Res.*, 106, 31597–31609.
829
830 Lam, P. J., Bishop, J.K.B. (2007) High biomass low export regimes in the southern ocean.
831 *Deep-Sea Res. (2 Top. Stud. Oceanogr.)*, **54** (5–7), 601–638
832
833 Lampitt, R.S., Antia, A.N. (1997) Particle flux in deep seas: regional characteristics and
834 temporal variability. *Deep-Sea Res. (1 Oceanogr. Res. Pap.)*, **44** (8): 1377–1403.
835
836 Laubscher, R.K., Perissinotto, R. and McQuaid, C.D. (1993) Phytoplankton production
837 and biomass at frontal zones in the Atlantic Sector of the Southern Ocean. *Polar Biol.*,
838 **13**, 471–481.

839

840 Leventer, A., Dunbar, R.B. (1987) Diatom flux in McMurdo Sound, Antarctica. *Mar.*
841 *Micropaleontol.*, **12**, 49–64.

842

843 Leventer, A., Dunbar, R.B., DeMaster, D.J. (1993) Diatom Evidence for Late Holocene
844 Climatic Events in Granite Harbor, Antarctica. *Paleoceanography* **8**, 373-386.

845

846 Leventer, A., Dunbar, R.B., (1996) Factors influencing the distribution of diatoms and
847 other algae in the Ross Sea. *J. Geophys. Res.*, **101**, 18489–500.

848

849 Locarnini, R.A., Mishonov, A.V. and Antonov, J.I. (2010) *World Ocean Atlas 2009*,
850 Volume 1: Temperature. Vol. 1, U.S. Government Printing Office, Washington, D.C.

851

852 Massom, R., Reid, P., Stammerjohn, S., *et al.* (2013) Change and Variability in East
853 Antarctic Sea Ice Seasonality, 1979/80–2009/10. *Plos one* **8** (5), e64756.

854

855 Martin, J.H., Fitzwater, S.E., Gordon, R. M. (1990) Iron deficiency limits phytoplankton
856 growth in Antarctic waters. *Global Biogeochem. Cycles* **4**, 5-12.

857

858 Matsumoto K., Sarmiento J.L. and Brzezinski M.A. (2002) Silicic acid leakage from the
859 Southern Ocean: A possible explanation for glacial atmospheric pCO2. *Global*
860 *Biogeochem. Cycles*, **16**, 1031.

861

862 Moore, J.K., Abbott, M.R. (2000) Phytoplankton chlorophyll distributions and primary
863 production in the Southern Ocean. *J. Geophys. Res.*, **105**, 28709–28722.

Nelson, D.M., Tréguer, P., Brzezinski, M.A., *et al.* (1995) Production and dissolution of biogenic silica in the ocean: Revised global estimates, comparison with regional data and relationship to biogenic sedimentation. Global Biogeochem. Cycles, 9, 359–372.

Orsi, A.H., Whitworth III, T., Nowlin Jr., W.D. (1995) On the meridional extent and fronts of the Antarctic Circumpolar Current. *Deep-Sea Res. (1 Oceanogr. Res. Pap.)*, **42**, 641–673.

Ortiz, J.D., Mix, A.C. (1997) Comparison of Imbrie-Kipp transfer function and modern analog temperature estimates using sediment trap and core top foraminiferal faunas. *Paleoceanography*, **12**, 175–190.

Parslow, J., Boyd, P., Rintoul, S.R. *et al.* (2001) A sub-surface chlorophyll maximum in the Polar Frontal Zone south of Australia: seasonal evolution and implications for phytoplankton-light-nutrient interactions. *J. Geophys. Res.*, **106**, 31543–31550.

Pilskaln, C.H., Manganini, S.J., Trull, T., *et al.* (2004) Geochemical particle fluxes in the Southern Indian Ocean seasonal ice zone: Prydz Bay region, east Antarctica. *Deep-Sea Res. (1 Oceanogr. Res. Pap.)*, **50**, 307–32.

Pondaven, P., Ragueneau, O., Tréguer, P., *et al.* (2000) Resolving the `opal paradox' in the Southern Ocean. *Nature*, **405**, 168–172.

888 Popp, B.N., Trull, T., Kenig, F. *et al.* (1999) Controls on the carbon isotopic composition
889 of Southern Ocean phytoplankton. *Global Biogeochem. Cycles* **13** (4), 827–843.
890
891 Quéguiner, B. (2013) Iron fertilization and the structure of planktonic communities in
892 high nutrient regions of the Southern Ocean. *Deep-Sea Res. (1 Oceanogr. Res. Pap.)*I,
893 **90**, 43-54.
894
895 Quilty, P., Kerry, K.R., Marchant, H.J. (1985) A seasonally recurrent patch of Antarctic
896 planktonic diatoms. *Search (ANZAAS)*, **16**, 48.
897
898 Reynolds, R.W., Rayner, N.A., Smith, T.M. *et al.* (2002) An improved in situ and satellite
899 SST analysis for climate. *J. Climate*, **15**, 1609–1625.
900
901 Rintoul, S.R., Bullister, J.L. (1999) A late winter Hydrographic section from Tasmania to
902 Antarctica. *Deep-Sea Res. (1 Oceanogr. Res. Pap.)*, **46**, 1417–1454.
903
904 Rintoul, S.R., Sokolov, S. (2001) Baroclinic transport variability of the Antarctic
905 Circumpolar Current south of Australia (WOCE repeat section SR3). *J. Geophys. Res.*
906 **106**, 2795–2814.
907
908 Romero, O., Armand, L.K., Crosta, X. *et al.* (2005) The biogeography of major diatom
909 taxa in Southern Ocean sediments: 3. Tropical/Subtropical species. *Palaeogeogr.,*
910 *Palaeoclimatol., Palaeoecol.*, **223**, 49–65.
911

912 Romero, O.E., Fischer, G., Lange, C.B. *et al.*(2000) Siliceous phytoplankton of the
913 western equatorial Atlantic: sediment traps and surface sediments. *Deep-Sea Res. (2*
914 *Top. Stud. Oceanogr.)* **47**, 1939–1959.
915
916 Romero, O.E., Lange, C.B., Fischer, *et al.* (1999). Variability in export production
917 documented by downward fluxes and species composition of marine planktonic
918 diatoms: observations from the tropical and equatorial Atlantic. In: Fischer, G., Wefer,
919 G. (Eds.), The Use of Proxies in Paleoceanography, Examples from the South Atlantic.
920 Springer, Berlin, Heidelberg, pp. 365–392.
921
922 Romero, O., Thunell, R.C., Astor, Y., et al. (2009) Seasonal and interanual dynamics in
923 diatom production in the Cariaco Basin, Venezuela. *Deep-Sea Res. (1 Oceanogr. Res.*
924 *Pap.)*, **56**, 571–581.
925
926 Sakshaug, E., Holm-Hansen, O. (1984) Factors governing pelagic production in polar
927 oceans. In: Holm-Hansen, O., Bolis, L., Gilles, R. (Eds.), *Marine Phytoplankton and*
928 *Productivity. Lecture Notes on Coastal and Estuarine Studies*, vol. 8. Springer, Berlin,
929 pp. 1–18.
930
931 Sancetta, C., Calvert, S.E. (1988) The annual cycle of sedimentation in Saanich Inlet,
932 British Columbia: implications for the interpretation of diatom fossil assemblages. *Deep*
933 *Sea Res.* **35** (1), 71–90
934
935 Sarmiento, J.L., T.M.C. Hughes, R.J. Stouffer *et al.* (1998) Simulated response of the
936 ocean carbon cycle to anthropogenic climate warming, *Nature*, **393**, 245–249.

937

938 Schrader, H. J., Gersonde, R. (1978) Diatoms and silicofagellates. Micropaleontological
939 counting methods and techniques: an exercise on an eight metres section of the Lower
940 Pliocene of Capo Rosello, Sicily. *Utrecht Bull. Micropaleontol*. **17**, 129–176.

941

942 Semina, H.J. (2003) SEM-studied diatoms of different regions of the World Ocean.
943 Iconographia Diatomologica **10**, 1– 362.

944

945 Smetacek, V. (1985) Role of sinking in diatom life-history cycles: ecological,
946 evolutionary and geological significance. *Mar. Biol.* **84**, 239-251.

947

948 Smetacek, V. (1999). Diatoms and the ocean carbon cycle. *Protist*, **250**, 25– 32

949

950 Smetacek, V., Assmy, P., Henjes, J. (2004) The role of grazing in structuring Southern
951 Ocean pelagic ecosystems and biogeochemical cycles. *Antarctic Science*, **16**: 541–558.

952

953 Smith Jr., W.O., Nelson, D.M. (1986) Importance of ice edge phytoplankton production
954 in the Southern Ocean. *Bioscience* **36** (4), 251–257.

955

956 Smith Jr., K.L., Sherman, A.D., Shaw, T.J. *et al.* (2011) Carbon export associated with
957 free-drifting icebergs in the Southern Ocean. *Deep-Sea Res. (2 Top. Stud. Oceanogr.)*
958 **58**, (11–12), 1485–1496.

959

960 Sohrin, Y., Iwamoto, S., Matsui, M. *et al.* (2000) The distribution of Fe in the Australian
961 sector of the Southern Ocean. *Deep-Sea Res. (1 Oceanogr. Res. Pap.)*, **47,** 55–84.

962

963 Sokolov, S., Rintoul, S.R. (2002) Structure of southern ocean fronts at 140 E. *J. Mar.*
964 *Syst.* **37**, 151–184.

965

966 Sokolov, S., Rintoul, S.R. (2007) Multiple Jets of the Antarctic Circumpolar Current
967 South of Australia. *J. Physical Oceanogr.*, **37**, 1394–1412

968

969 Sokolov, S., Rintoul, S.R. (2009a) Circulation structure and distribution of the Antarctic
970 Circumpolar Current fronts: 1. Mean circumpolar paths. *J. Geophys. Res.* **114**, C11018.

971

972 Sokolov, S., Rintoul, S.R. (2009b) Circulation structure and distribution of the Antarctic
973 Circumpolar Current fronts: 2. Variability and relationship to sea surface height. J.
974 *Geophys. Res.* **114**, C11019.

975

976 Sullivan, C.W., McClain, C.R., Comiso, J.C., Smith, W.O. (1988) Phytoplankton standing
977 crops within an Antarctic ice edge assessed by satellite remote sensing. *J. Geophys. Res.*
978 **93**, 12487–12498.

979

980 Suzuki, H., Sasaki, H., Fukuchi, M. (2001) Short-term variability in the flux of rapidly
981 sinking particles in the Antarctic Marginal Ice Zone. *Polar Biol.* **24**, 697–705.

982

983 Takahashi, K. (1986) Seasonal fluxes of pelagic diatoms in the subarctic Pacific, 1982–
984 1983. Deep-Sea Res. **33**, 1225–51.

985

Taylor, F., Sjunneskog, C. (2002) Postglacial marine diatom record of the Palmer Deep, Antarctic Peninsula (ODP Leg 178, Site 1098) 2. Diatom assemblages. *Paleoceanography* **17**, PAL 2-1-PAL 2-12.

Tréguer, P. J., De La Rocha, C. L. (2013) The world ocean silica cycle. *Annual review of marine science*, 5, 477-501.

Trull, T., Armand, L. (2001) Insights into Southern Ocean Carbon export from the δ 13 C of particles and dissolved inorganic carbon during the SOIREE iron release experiment. *Deep-Sea Res. (2 Top. Stud. Oceanogr.)*, **48**, 2655–2680.

Trull, T., SedwickF, P.N., Griffiths, F.B. et al. (2001a) Introduction to special section: SAZ Project. *J. Geophys. Res.*, **106**, 31425–31429.

Trull, T., Bray, S., Manganini, S., *et al.* (2001b) Moored sediment trap measurements of carbon export in the Subantarctic and Polar Frontal Zones of the Southern Ocean, south of Australia, *J. Geophys. Res.*, **106**, 31489–31510.

Trull, T., Rintoul, S. R., Hadfield, M., *et al.* (2001) Circulation and seasonal evolution of polar waters south of Australia: Implications for iron fertilization of the Southern Ocean, *Deep-Sea Res. (1 Oceanogr. Res. Pap.)*, **48**, 2439–2466

Varela, D.E., Pride, C.J., Brzezinski, M.A. (2004) Biological fractionation of silicon isotopes in Southern Ocean surface waters. Global Biogeochem. Cy., **18**, GB1047.

1011 Wefer, G., Fischer, G., F. Utterer, D. *et al.* (1988) Seasonal particle flux in the Bransfield
1012 Strait, Antarctica. *Deep-Sea Res. (1 Oceanogr. Res. Pap.)* **35** (6), 891–898.
1013
1014 Yu, E.F., Francois, R., Bacon, M.P. *et al.* (2001) Trapping efficiency of bottom-tethered
1015 sediment traps estimated from the intercepted fluxes of ^{230}Th and ^{231}Pa *Deep-Sea Res.*
1016 *(1 Oceanogr. Res. Pap.)*, **48** (3) 865–889.
1017
1018 Zeldis, J. (2001) Mesozooplankton community composition, feeding, and export
1019 production during SOIREE. *Deep-Sea Res. (2 Top. Stud. Oceanogr.)*, 48, 2615–2634.
1020

Table(s)

Click here to download Table(s): Table 1.eps

61_2000	Sampling period	Length	Total Mass Flux	$BSiO_2$		$CaCO_3$		POC		POC/PN	Diatoms
Cup	mid point	days	mg m^{-2} d^{-1}	mg m^{-2} d^{-1}	%	mg m^{-2} d^{-1}	%	mg m^{-2} d^{-1}	%	molar ratio	10^6 valves m^{-2} d^{-1}
1	Nov. 30, 2001	8	48	26	54	14	30	0.7	1.5	6.6	-
2	Dec. 08, 2001	8	78	47	61	17	22	1.7	2.2	6.1	9
3	Dec. 16, 2001	8	326	198	61	62	19	6.9	2.1	5.4	82
4	Dec. 24, 2001	8	509	326	64	140	28	6.4	1.3	3.5	85
5	Jan. 01, 2002	8	1151	856	74	44	4	26.9	2.3	7.4	408
6	Jan. 09, 2002	8	1069	796	75	170	16	14.8	1.4	4.9	200
7	Jan. 17, 2002	8	656	478	73	60	9	11.3	1.7	6.1	159
8	Jan. 25, 2002	8	702	541	77	38	5	11.0	1.6	6.1	296
9	Feb. 02, 2002	8	666	520	78	39	6	12.0	1.8	6.5	184
10	Feb. 10, 2002	8	595	469	79	24	4	8.2	1.4	6.2	295
11	Feb. 18, 2002	8	534	425	80	20	4	6.2	1.2	6.5	149
12	Feb. 26, 2002	8	524	418	80	19	4	4.7	0.9	6.5	152
13	Mar. 06, 2002	8	586	471	80	15	3	6.9	1.2	7.2	120
14	Mar. 14, 2002	8	285	230	81	11	4	3.2	1.1	6.6	71
15	Mar. 22, 2002	8	290	253	87	7	3	3.2	1.1	6.8	66
16	Mar. 30, 2002	8	263	218	83	8	3	2.6	1.0	6.1	87
17	Apr. 08, 2002	10	264	220	83	7	3	2.2	0.8	6.4	97
18	May. 08, 2002	50	130	102	78	5	4	1.2	1.0	5.9	47
19	Jun. 29, 2002	54	65	52	79	2	4	0.7	1.0	6.6	10
20	Aug. 22, 2002	55	56	44	78	2	4	0.8	1.5	6.6	19
21	Sep. 29, 2002	20	42	34	81	2	4	0.5	1.3	7.2	6
Annualised values			**232**	**178**	**76**	**17**	**7.4**	**3.3**	**1.4**	**6.1**	**67**
Annual flux			**85 g m^{-2} y^{-1}**	**65 g m^{-2} y^{-1}**		**6 g m^{-2} y^{-1}**		**1.2 g m^{-2} y^{-1}**			**24 10^9 valves m^{-2} y^{-1}**

61_3700	Sampling period	Length	Total Mass Flux	$BSiO_2$		$CaCO_3$		POC		POC/PN	Diatoms
Cup	mid point	days	mg m^{-2} d^{-1}	mg m^{-2} d^{-1}	%	mg m^{-2} d^{-1}	%	mg m^{-2} d^{-1}	%	molar ratio	10^6 valves m^{-2} d^{-1}
1	Nov. 30, 2001	8	38	25	64	9	23	0.4	1.1	7.4	-
2	Dec. 08, 2001	8	31	17	54	9	28	0.4	1.2	6.4	-
3	Dec. 16, 2001	8	99	51	52	29	30	1.4	1.4	6.7	4
4	Dec. 24, 2001	8	231	148	64	59	26	1.4	0.6	2.6	12
5	Jan. 01, 2002	8	873	656	75	87	10	17.3	2.0	6.8	118
6	Jan. 09, 2002	8	1157	886	77	154	13	19.8	1.7	6.9	479
7	Jan. 17, 2002	8	828	611	74	166	20	9.4	1.1	4.6	354
8	Jan. 25, 2002	8	490	376	77	34	7	6.4	1.3	6.4	169
9	Feb. 02, 2002	8	491	384	78	32	6	6.5	1.3	6.1	385
10	Feb. 10, 2002	8	419	335	80	19	4	6.0	1.4	7.0	281
11	Feb. 18, 2002	8	584	475	81	36	6	6.2	1.1	6.2	254
12	Feb. 26, 2002	8	581	473	81	31	5	5.2	0.9	5.5	238
13	Mar. 06, 2002	8	849	737	87	23	3	7.6	0.9	6.5	326
14	Mar. 14, 2002	8	369	233	63	18	5	3.3	0.9	6.5	44
15	Mar. 22, 2002	8	218	174	80	8	4	2.6	1.2	7.3	32
16	Mar. 30, 2002	8	258	198	77	10	4	2.5	1.0	7.2	43
17	Apr. 08, 2002	10	257	202	79	9	3	2.3	0.9	6.9	32
18	May. 08, 2002	50	118	98	83	5	4	1.2	1.0	6.3	8
19	Jun. 29, 2002	54	0	0	83	0	4	0.0	1.0	6.3	-
20	Aug. 22, 2002	55	0	0	83	0	4	0.0	1.0	6.3	-
21	Sep. 29, 2002	20	0	0	83	0	4	0.0	1.0	6.3	-
Annualised values			**188**	**146**	**78**	**17**	**9**	**2.3**	**1.2**	**6.2**	**62**
Annual flux			**69 g m^{-2} y^{-1}**	**53 g m^{-2} y^{-1}**		**6 g m^{-2} y^{-1}**		**0.9 g m^{-2} y^{-1}**			**23 10^9 valves m^{-2} y^{-1}**

Table 1

2000 m	Total Mass Flux	$BSiO_2$	$CaCO_3$	POC
Total Mass Flux	-			
$BSiO_2$	0.99	-		
$CaCO_3$	0.37	0.30	-	
POC	0.86	0.83	0.24	-

3700 m	Total Mass Flux	$BSiO_2$	$CaCO_3$	POC
Total Mass Flux	-			
$BSiO_2$	0.99	-		
$CaCO_3$	0.61	0.54	-	
POC	0.87	0.83	0.63	-

Table 2

Table(s)

Click here to download Table(s): Table 3.eps

	2000m		3700 m
	Average 309 days	Average 172 days	Average 172 days
Actinocyclus spp.	0.01	0.01	0.03
Actinocyclus actinochilus (Ehrenberg) Simonsen	0.02	0.01	0.00
Asteromphalus hookeri Ehrenberg	0.17	0.20	0.48
A. hyalinus Karsten	0.16	0.26	0.29
A. parvulus Karsten	0.19	0.32	0.35
Asteromphalus spp.	0.01	0.01	0.01
Azpeitia tabularis (Grunow) Fryxell et Sims	0.68	0.57	0.74
Chaetoceros aequatorialis var. *antarcticus* Manguin	0.02	0.03	0.06
Ch. atlanticus Cleve	0.16	0.29	0.37
Ch. dichaeta Ehrenberg	0.11	0.19	0.16
Ch. peruvianus Brightwell	0.00	0.00	0.01
Chaetoceros sp. A	0.08	0.14	0.11
Chaetoceros sp. B	0.07	0.13	0.19
Chaetoceros spp.	0.15	0.27	0.32
Chaetoceros Hyalochaete resting spores	0.14	0.25	0.14
Corethron spp.	0.01	0.01	0.00
Dactyliosolen antarcticus Castracane			
Eucampia antarctica (Castracane) Mangin	0.13	0.14	0.20
Fragilariopsis curta (Van Heurck) Hustedt	0.57	1.00	1.11
F. cylindrus (Grunow) Krieger	0.16	0.29	0.10
F. kerguelensis (O'Meara) Hustedt	79.91	72.41	68.34
F. obliquecostata (van Heurck) Heiden	0.02	0.03	0.05
F. pseudonana (Hasle) Hasle	2.03	3.64	1.43
F. rhombica (O'Meara) Hustedt	0.93	1.58	2.13
F. ritscheri Hustedt	0.07	0.13	0.11
F. separanda Hustedt	2.10	2.85	2.03
F. cf. *sublineata* (Van Heurck) Heiden	0.03	0.04	0.03
Haslea trompii (Cleve) Simonsen	0.01	0.01	0.02
Navicula directa (Smith) Ralfs in Pritchard	0.33	0.58	1.06
N. sicula var. *bicuneata* (Castracane) Grunow	0.06	0.10	0.14
Pleurosigma directum Grunow in Van Heurck	0.02	0.03	0.03
Pseudo-nitzschia < 3 µm transapical axis	0.40	0.72	1.41
P-n. heimii Manguin	0.01	0.02	0.02
Pseudo-nitzschia spp.	0.11	0.19	0.08
Porosira pseudodenticulata (Hustedt) Jousé	0.02	0.03	0.03
Proboscia spp.	0.00	0.00	0.01
Rhizosolenia antennata (Ehrenberg) Brown f. *semispina* Sundström	0.00	0.00	0.02
Rhizosolenia bergonii Peragallo	0.00	0.00	0.02
Rhizosolenia sp. f. 1A (Armand et Zielinski)	0.01	0.01	0.02
Rhizosolenia spp.	0.09	0.07	0.02
Thalassionema nitzschioides f. *capitulata* (Castracane) Moreno-Ruiz	0.06	0.09	0.11
T. nitzschioides f. *lanceolata* (Grunow) Pergallo et Pergallo	0.05	0.02	0.02
Stellarima stellaris (Roper) Hasle et Sims	0.00	0.00	0.02
Thalassiosira gravida Cleve	0.03	0.05	0.11
T. gracilis var. *gracilis* (Karsten) Hustedt	3.65	6.08	7.41
T. gracilis var. *expecta* (Van Landingham) Frxyell et Hasle	0.42	0.65	1.30
T. lentiginosa (Janisch) Fryxell	4.97	4.63	6.77
T. maculata Fryxell et Johansen	0.05	0.02	0.02
T. oestrupii (Ostenfeld) Hasle	0.01	0.02	0.01
T. oliveriana (O'Meara) Makarova et Nikolaev	0.67	0.37	0.42
T. tumida (Janisch) Hasle	0.12	0.07	0.10
T. leptopus (Grunow ex Van Heurck) Hasle et G.Fryxell	0.01	0.01	0.54
T. lineata Jousé	0.11	0.14	0.36
Thalassiosira spp. < 20 µm	0.37	0.62	0.29
Thalassiosira spp. > 20 µm	0.04	0.05	0.00
Thalassiosira sp. A	0.18	0.22	0.01
Thalassiosira sp. B	0.02	0.03	0.08
Thalassiothrix antarctica Schimper ex Karsten	0.20	0.18	0.58
Tropidoneis group	0.04	0.05	0.12
Other centrics	0.07	0.07	0.02
Other pennates	0.01	0.01	0.01

Table 3

Figure(s)

Click here to download Figure(s): Fig. 1. Black and white.eps

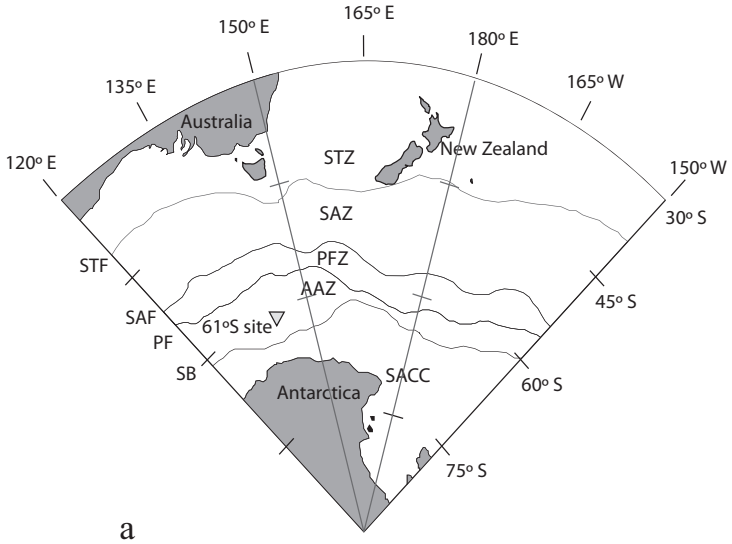

a

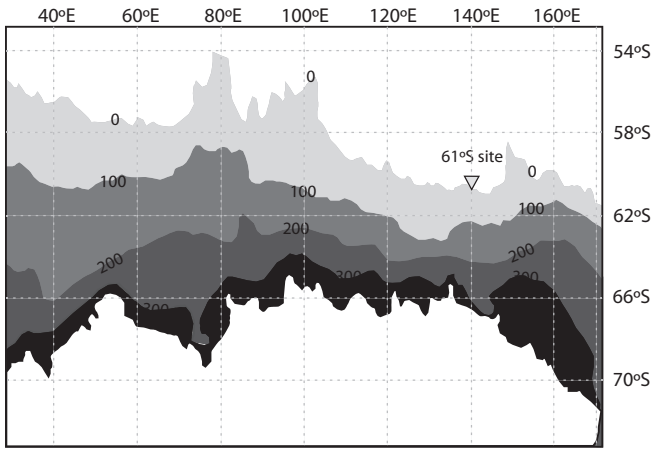

b

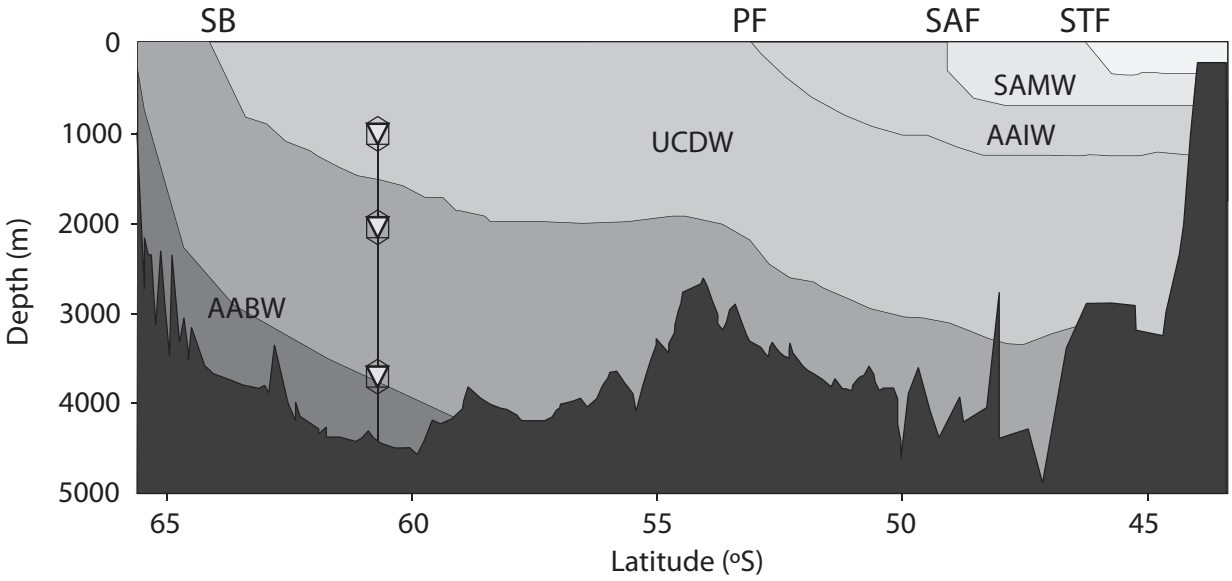

c

Figure 1

Figure(s)

Click here to download Figure(s): Fig. 1. Colour.eps

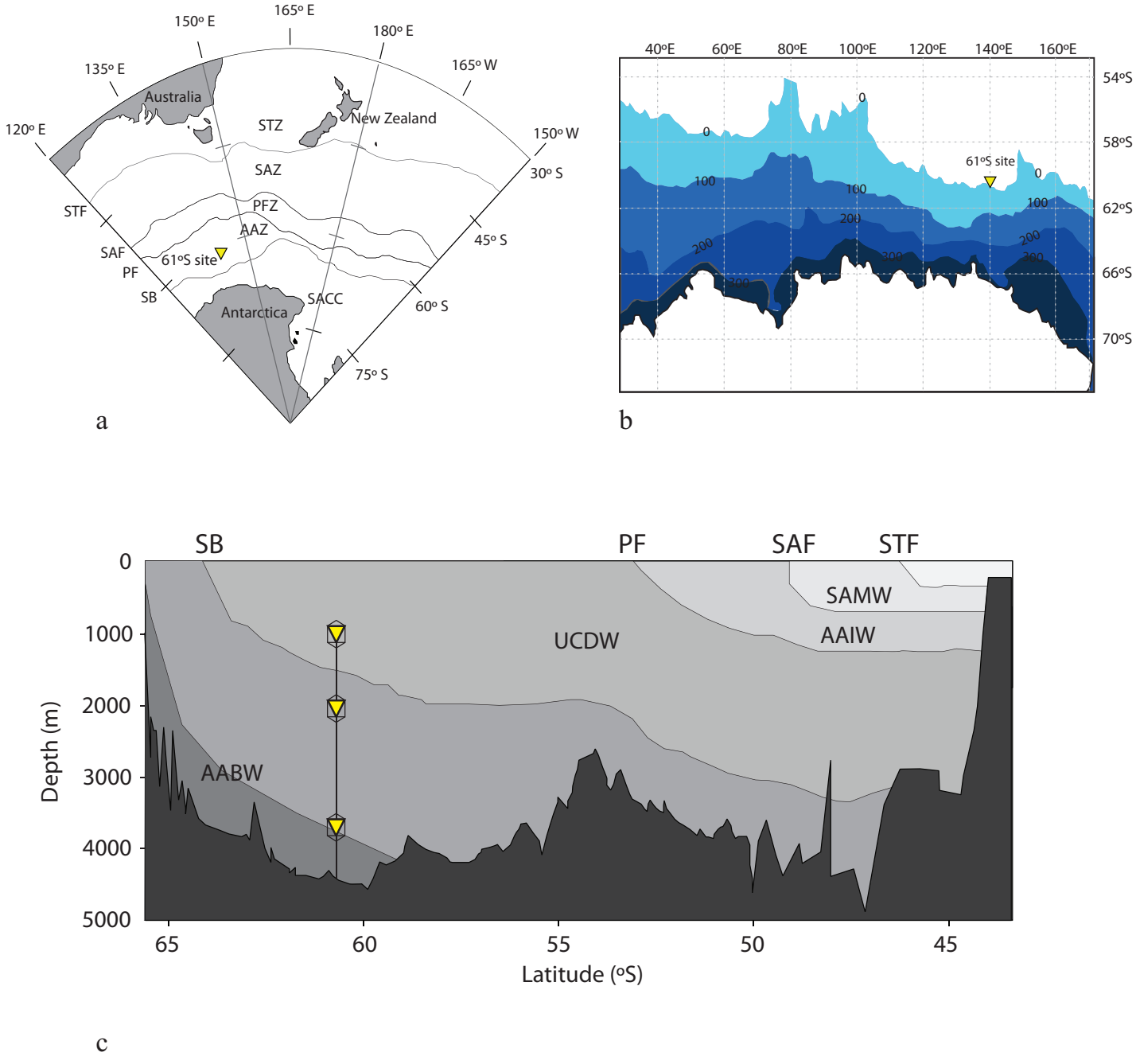

Figure 1

Figure(s)

Click here to download Figure(s): Fig. 2. Black and white.eps

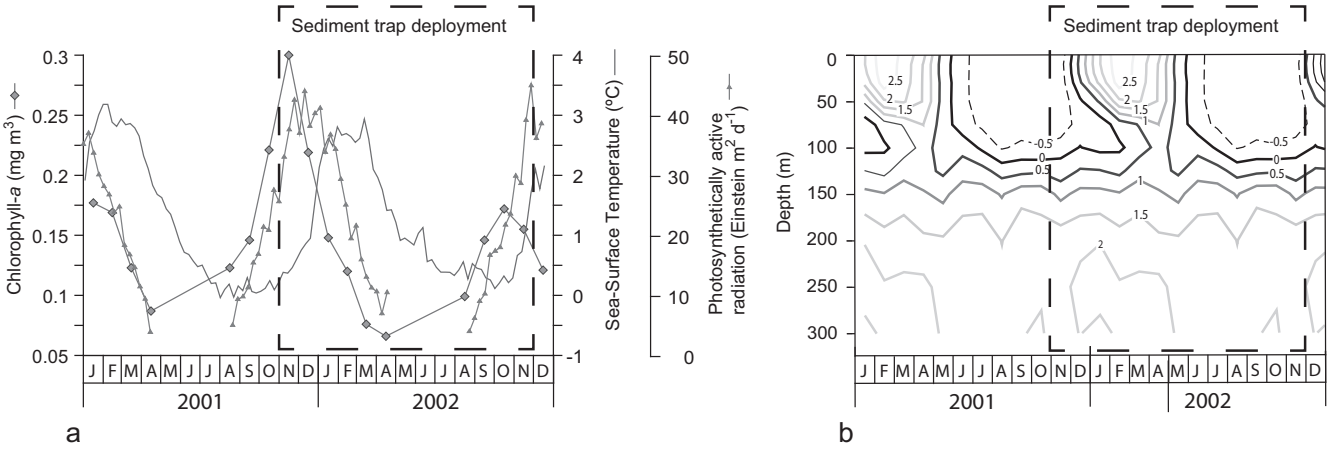

Figure 2

Figure(s)

Click here to download Figure(s): Fig. 2. Colour.eps

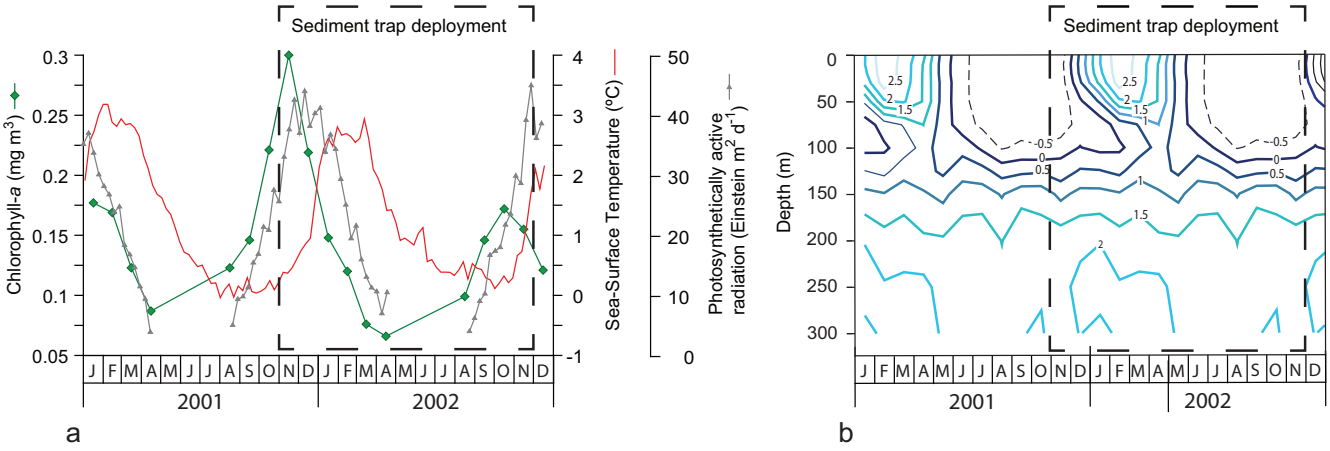

Figure 2

Figure(s)

Click here to download Figure(s): Fig. 3. Black and white.eps

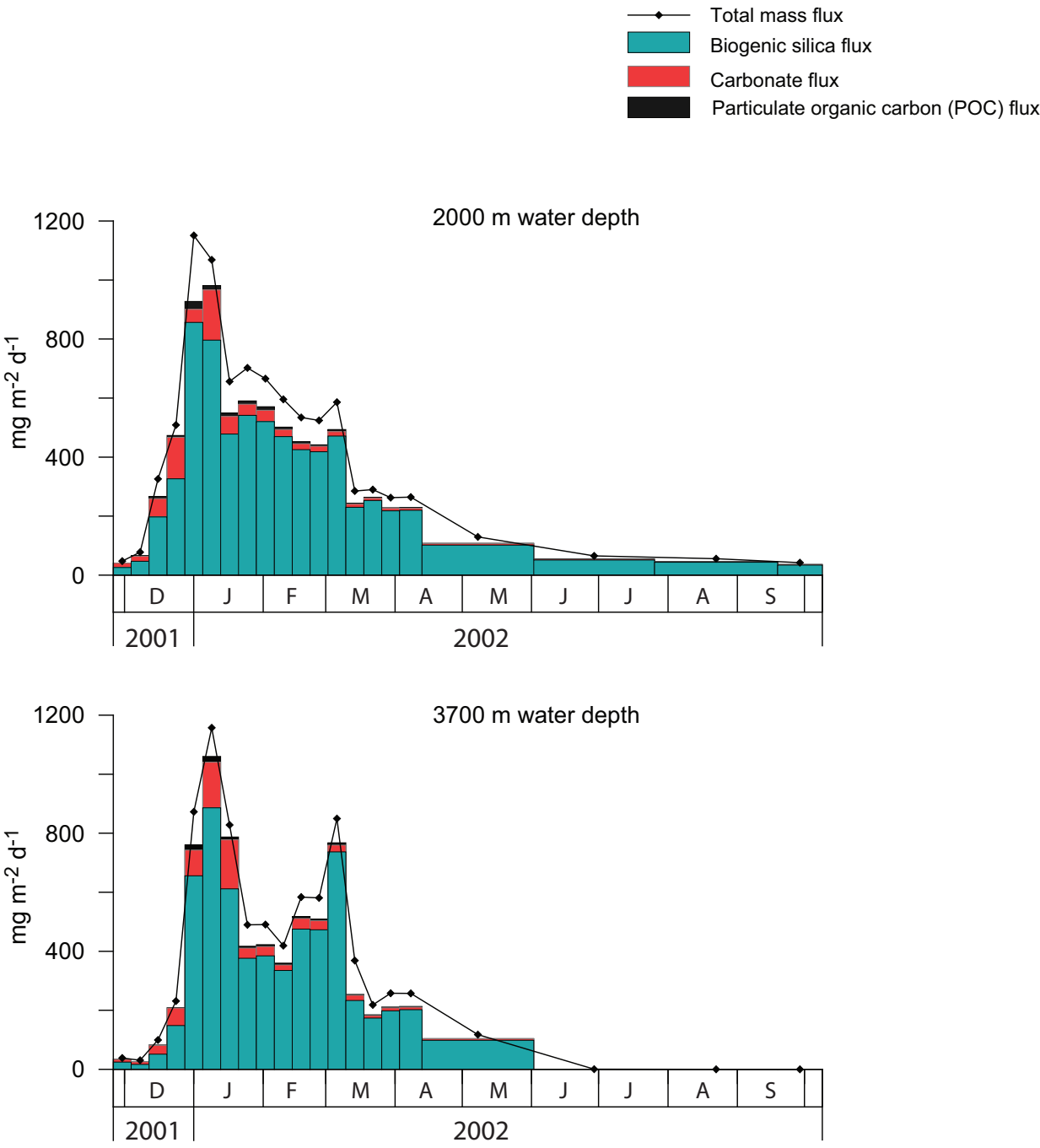

Figure 3

Figure(s)

Click here to download Figure(s): Fig. 3. Colour.eps

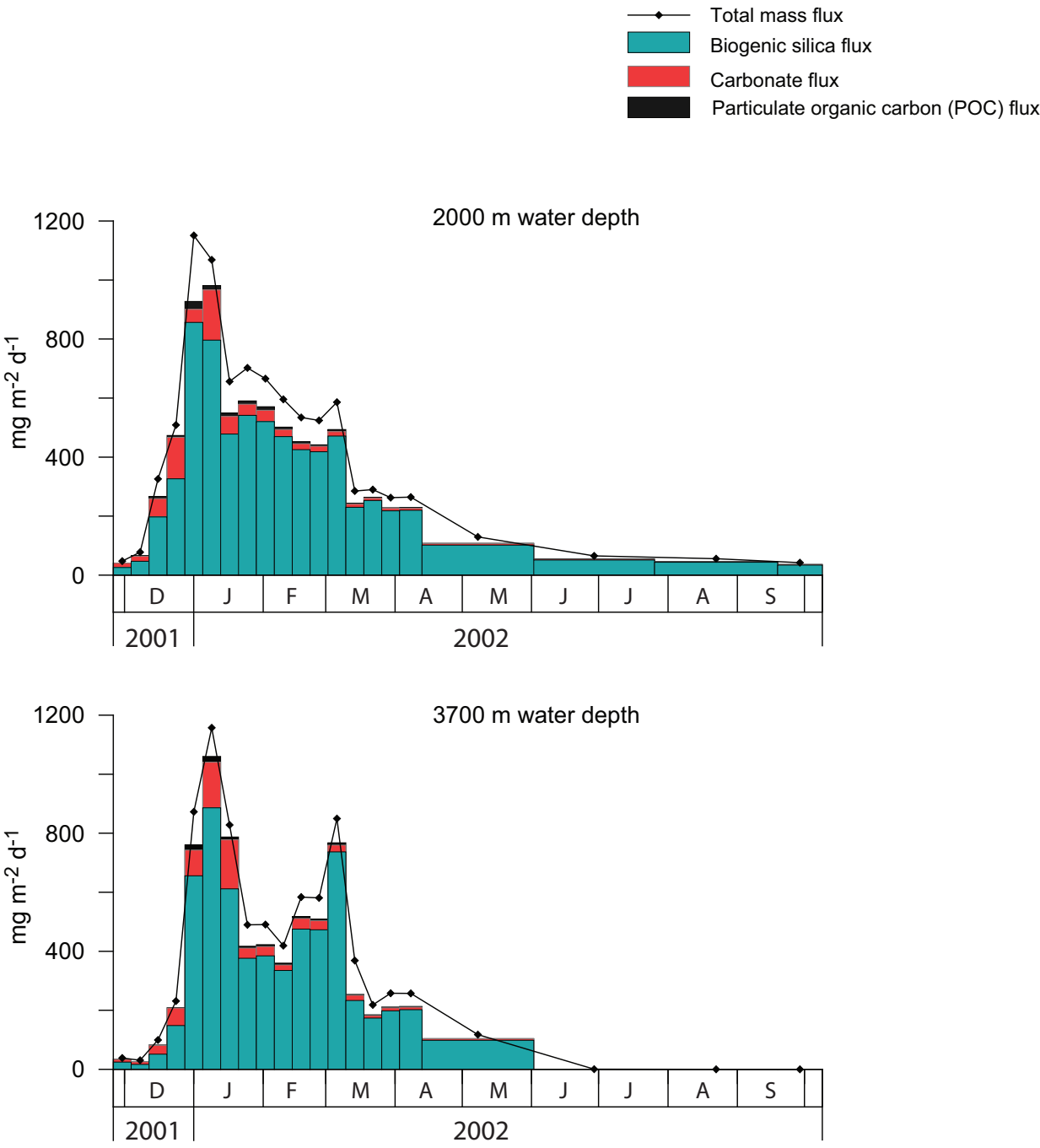

Figure 3

Figure(s)

Click here to download Figure(s): Fig. 4.eps

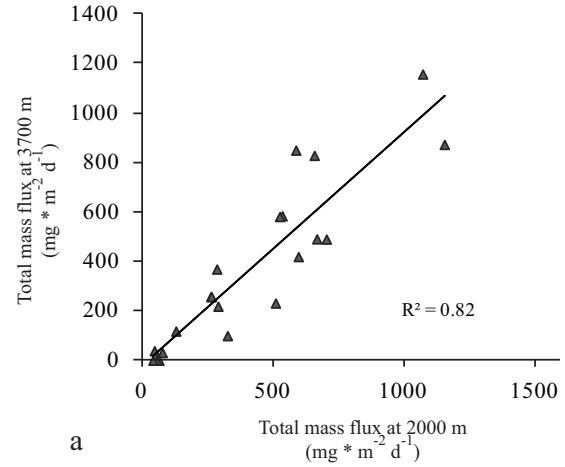

a

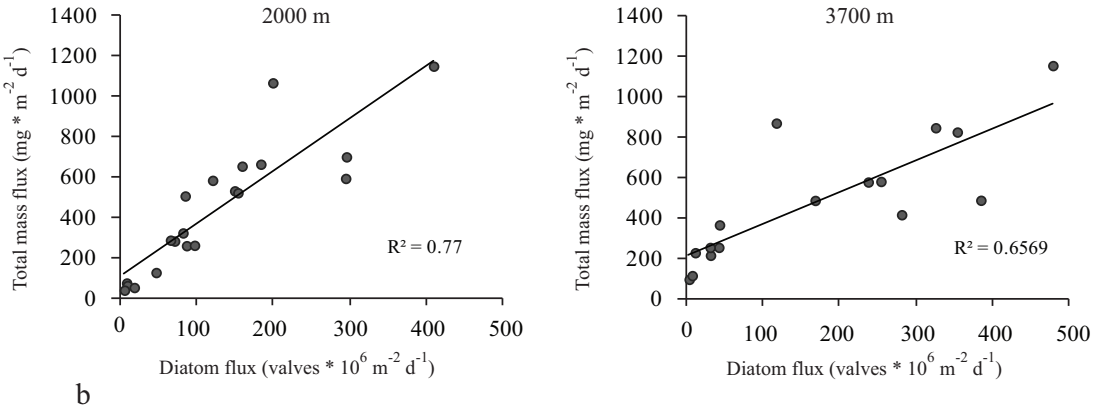

b

Figure 4

Figure(s)

Click here to download Figure(s): Fig. 5. Black and white.eps

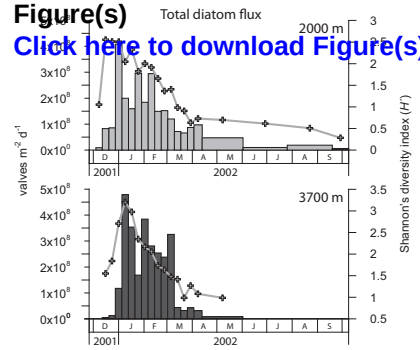

a

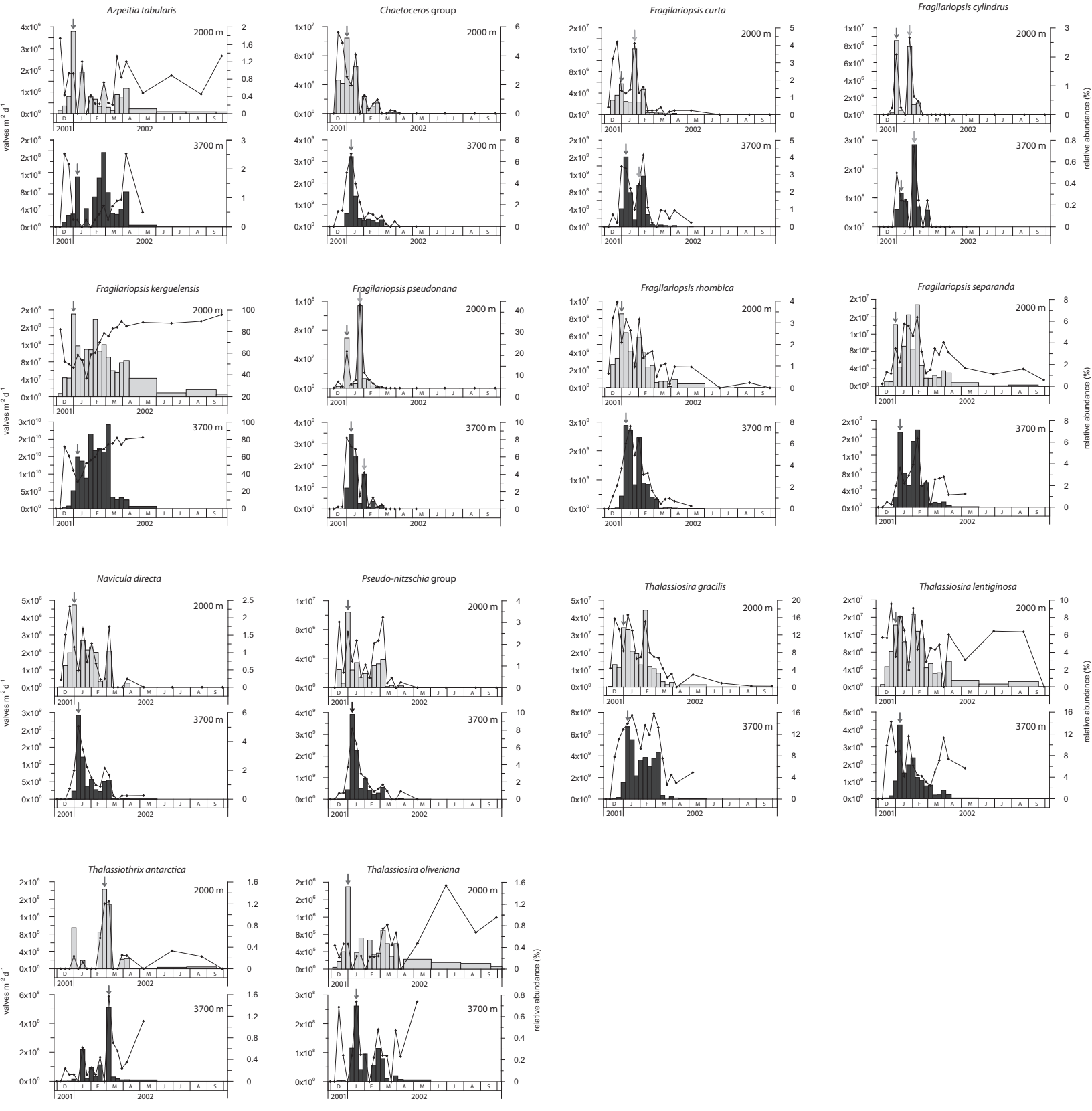

b

Figure(s)

Click here to download Figure(s): Fig. 5. Colour.eps

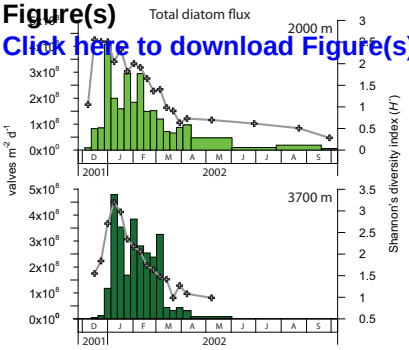

a

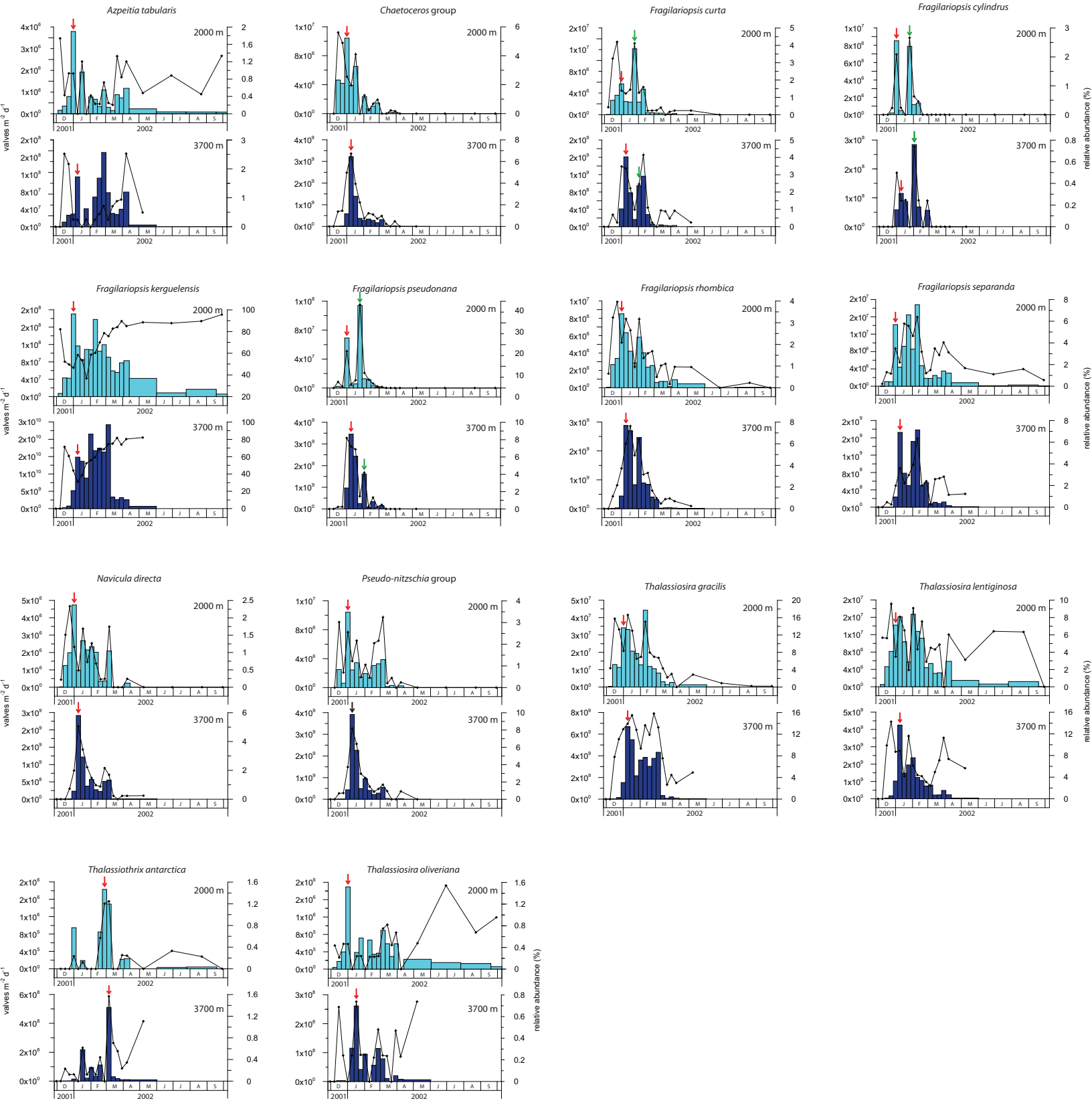

b

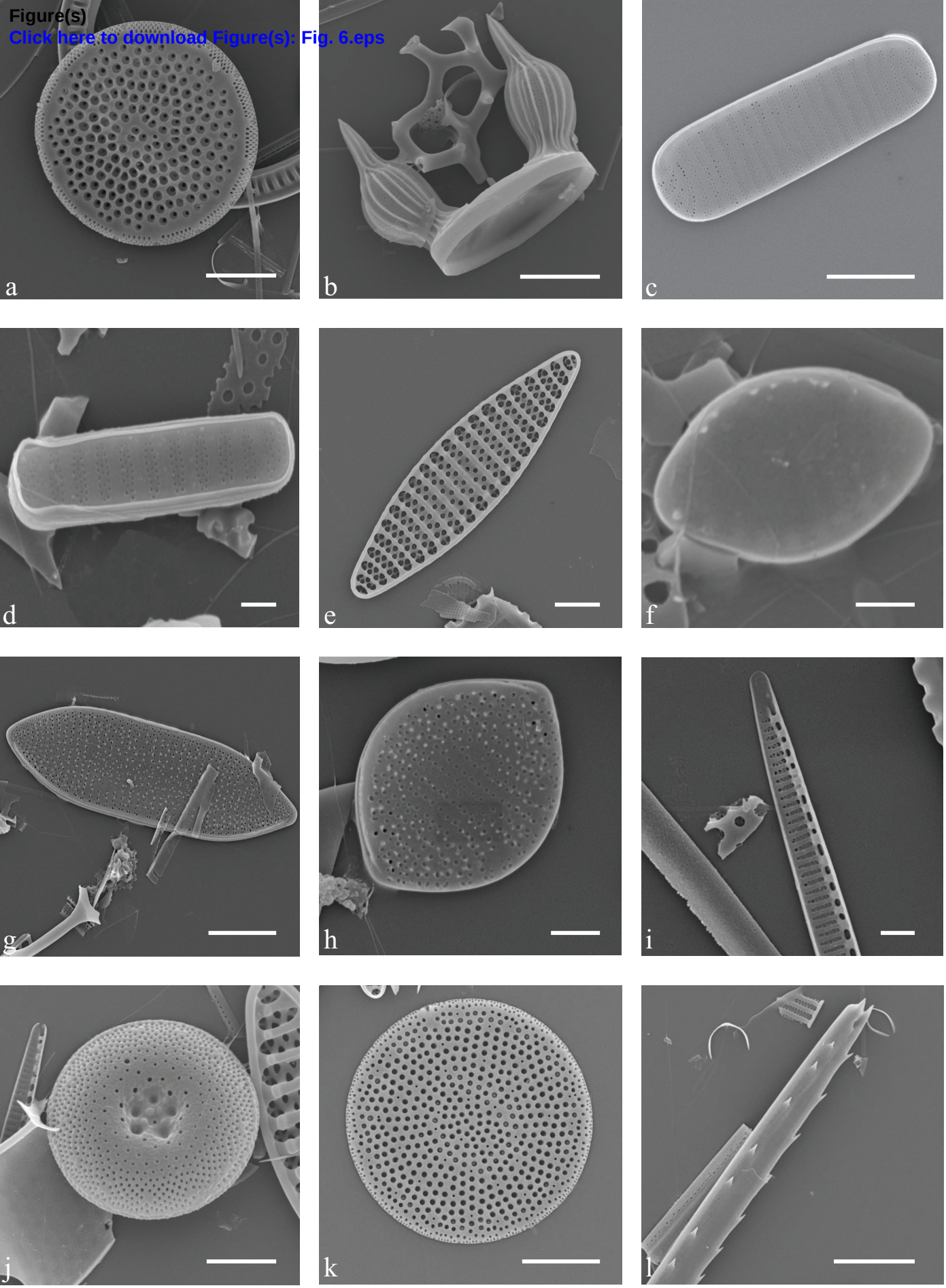

Figure 6